Beams-doc-4212

Design of the Advanced Superconducting Test Accelerator

Editor: Mike Church

Contributors: Kermit Carlson, Brian Chase, Mike Church, Jerzy Czajkowski, Nathan Eddy, Elvin Harms, Emil Huedem, Amber Johnson, Mike Kucera, Alex Lumpkin, Lucy Nobrega, Chris Prokop, John Reid, Jinhao Ruan, Jay Theilacker, Arden Warner

Nov. 21, 2012

Table of Contents

1 FACILITY OVERVIEW 4

2 ELECTRON GUN 7

2.1 DESCRIPTION 7
2.2 INITIAL PERFORMANCE 9

3 PHOTOCATHODE LASER 10

3.1 SYSTEM DESIGN 10
3.2 COMMISSIONING AND PRELIMINARY TESTS 11
3.2.1 Fiber based seed laser 11
3.2.2 Diode pumped multi-pass (MP) amplifier 12
3.2.3 Future development and additional laser systems 14

4 BEAMLINES 15

4.1 LOW ENERGY BEAMLINE LAYOUT 15
4.2 HIGH ENERGY BEAMLINE LAYOUT 15
4.3 MAGNETS 16
4.3.1 Low energy dipole correctors 16
4.3.2 Low energy quadrupoles 17
4.3.3 Low energy dipoles 17
4.3.4 High energy dipole correctors 18
4.3.5 High energy quadrupoles 18
4.3.6 High energy dipoles 19
4.3.7 Power supplies 19
4.4 VACUUM 20
4.5 DIAGNOSTICS OVERVIEW 20
4.6 BEAM DUMPS 21
4.6.1 Low energy beam dump 21
4.6.2 High energy beam dump 22

5 CRYOMODULES 25

5.1 DESCRIPTION 25
5.1.1 Capture cavities 1 & 2 (CC1, CC2) 26
5.1.2 Multi-cavity cryomodules (CM1, CM2, CM3, …) 28
5.2 INITIAL PERFORMANCE 31

6 RF SYSTEMS 37

6.1 HIGH LEVEL RF 37
6.2 LOW LEVEL RF 37
6.2.1 Field Control System 37
6.2.2 Resonance control system 38
6.2.3 Master Oscillator and Phase Reference Line 38

7 INSTRUMENTATION 40

7.1 BEAM POSITION MONITORS 40
7.2 WALL CURRENT MONITORS 40
7.3 BEAM PROFILE MONITORS 40

8 LATTICE CALCULATIONS AND SIMULATIONS 44

9 MACHINE PROTECTION SYSTEM 48

9.1 OVERVIEW 48
9.2 LASER PULSE CONTROLLER 50
9.3 FAST BEAM LOSS MONITORS 50
9.3.1 Loss Monitor Design and Specifications 51
9.3.2 Theory of operation 52
9.3.3 Beam Loss Monitor Test Results 53
9.3.4 Beam Loss Monitor Signal Processing 54
9.4 CRYOGENIC LOSS MONITORS 55

10 CONTROLS 57

10.1 TIMING 57

11 CRYOGENIC SYSTEM 60

12 ELECTRICAL POWER DISTRIBUTION 62

12.1 OVERVIEW 62
12.2 NML 62
12.3 CMTF 63

13 COOLING SYSTEMS 64

13.1 LOW CONDUCTIVITY WATER SYSTEMS 64
13.2 INDUSTRIAL COOLING WATER 68
13.3 HVAC 68

1 Facility overview

The Advanced Superconducting Test Accelerator (ASTA) is housed in the New Muon Lab (NML) building at Fermilab. It will be capable of testing 3 or more ILC-type SRF cryomodules under full ILC beam intensity and bunch structure. In addition, test beamlines and downstream beamlines will provide a venue for advanced accelerator R&D (AARD). The original NML building had been previously used for a high energy physics experiment, but has recently been repurposed to house ASTA [1.1]. The original footprint has been extended to accommodate high energy beamlines, a high energy beam dump, and an experimental area for AARD. Figure 1.1 shows a plan view of the upstream half of the facility, and Figure 1.2 shows a plan view of the downstream half.

The electron beam is produced by a 1.3 GHz RF photoinjector and then accelerated to ~50 MeV by two 1.3 GHz SRF cryomodules, each containing a single 9-cell cavity, before being injected into the 1st 8-cavity cryomodule. Initial beam commissioning of the cryomodule string will take place with a single Tesla type III+ cryomodule [1.2] driven by a 5 MW klystron. The next stage of commissioning will take place with two Tesla type III+ cryomodules and one ILC type IV cryomodule. This cryomodule string will be driven by a 10 MW multi-beam klystron, with its associated HV power supply, modulator, and waveguide distribution system. The high energy beamlines downstream of the cryomodules will provide transport to an AARD experimental area and to the high energy beam dump.

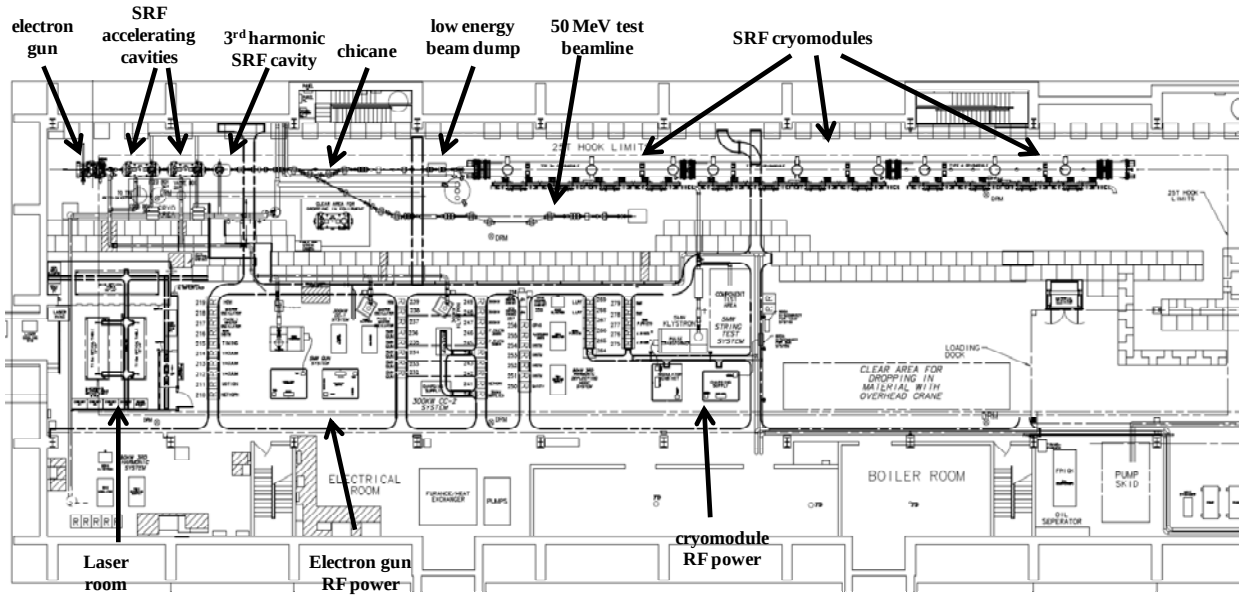

Figure 1.1: Upstream floor plan of the ASTA photoinjector and 3 SRF cryomodules in the original building footprint. The beamline is 1.2 m above the floor, the floor is 6.1 m below grade, and the building length is 74 m.

The cryogenic plant currently consists of 2 Tevatron-style satellite refrigerators capable of delivering 2°K helium but does not have the capacity to cool all 3 cryomodules at full beam intensity and at full pulse repetition rate. The Cryomodule Test Facility (CMTF) [1.1] is currently being built adjacent to NML and will provide the additional 2°K helium capacity

required to operate ASTA at full repetition rate, cryomodule test stands in CMTF, and the Project X Injection Experiment (PXIE).

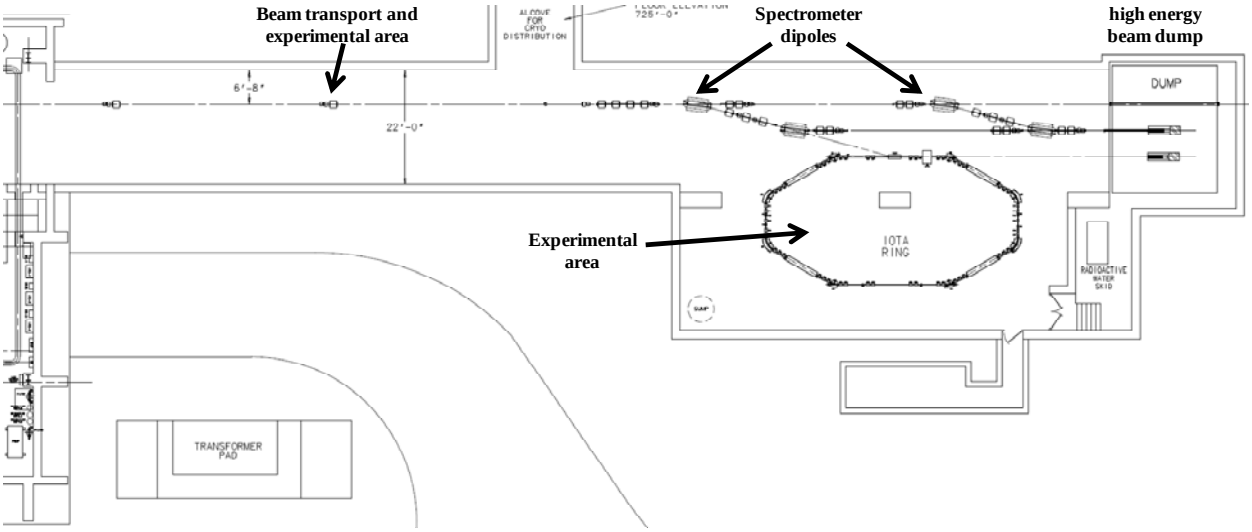

Figure 1.2: Downstream plan view of the ASTA high energy beamlines and experimental areas in the new underground tunnel. The tunnel extension is 70 m long. A service building is located above the experimental area.

The beam parameters for ASTA will have a wide range, depending on the particular application. Table 1.1 lists selected beam parameters for ILC-like conditions and the possible range for each parameter. As with all photoinjectors, many beam parameters are coupled, especially to the bunch intensity, because of space charge effects in the electron gun and low energy bunch compressor.

Table 1.1: Beam parameters for ASTA. The ILC-like parameter values are listed and also the range of each parameter.

parameter	ILC RF unit test	range	comments
bunch charge	3.2 nC	10's of pC to >20 nC	minimum determined by diagnostic thresholds; maximum determined by cathode QE and laser power
bunch spacing	333 nsec	<10 nsec to 10 sec	lower laser power at minimum bunch spacing
bunch train length	1 msec	1 bunch to 1 msec	maximum limited by modulator and klystron power
bunch train repetition rate	5 Hz	0.1 Hz to 5 Hz	minimum may be determined by egun temperature regulation and other stability considerations
norm. transverse emittance	~25 mm-mrad	<1 mm-mrad to >100 mm-mrad	maximum limited by aperture and beam losses; without bunch compression emittance is ~5 mm-mrad at 3.2 nC
RMS bunch length	1 ps	~10's of fs to ~10's of ps	minimum obtained with Ti:Sa laser; maximum obtained with laser pulse stacking
peak bunch current	3 kA	> 9 kA	3 kA based on Impact-Z simulations with low energy bunch compressor; 9 kA possible with 3.9 GHz linearizing cavity
injection energy	50 MeV	5 MeV to 50 MeV	may be difficult to transport 5 MeV beam to the dump; maximum determined by booster cavity gradients
high energy	820 MeV	50 MeV to 1500 MeV	radiation shielding limits the maximum; 1500 MeV with 6 cryomodules

References

[1.1] J. Leibfritz, *et al*., "Status and Plans for a SRF Accelerator Test Facility at Fermilab", MOP009 in NA-PAC'11, New York, NY, March 2011 (http://accelconf.web.cern.ch/AccelConf/PAC2011/papers/mop009.pdf)

[1.2] E. Harms, *et al.*, "RF Test Results from Cryomodule 1 at the Fermilab SRF Beam Test Facility", MOPO013 in 15th International Conf. on RF Superconductivity (SRF2011), Chicago, IL, July 2011; (http://lss.fnal.gov/archive/2011/conf/fermilab-conf-11-352-ad-td.pdf)

2 Electron gun

2.1 Description

The RF photocathode electron gun is identical to the guns recently developed at DESY Zeuthen (PITZ) for the FLASH facility [2.1]. It is a normal-conducting 1½ cell 1.3 GHz gun operated in $TM_{010,\pi}$ mode, with a Q_L of ~11,700, and driven by a 5 MW klystron. The power is coupled into the gun via a coaxial RF coupler at the downstream end of the gun. Five ceramic RF windows were purchased from Thales and have been conditioned to full power for both forward and reflected power. The gun is capable of average DC power dissipation of ~20 KW and requires a dedicated cooling water skid. A temperature feedback system will regulate cooling water temperature to better than ±0.02 °C for good phase stability. The gun will be routinely operated at peak gradients of 40-45 MV/m, and output beam kinetic energy of ~5 MeV. (For comparison, PITZ has successfully operated an identical gun at 60 MV/m for 700 μsec pulse lengths.) The peak gradient is given by E [MV/m] = 23.6 * sqrt(P [MW]) [2.2]. The photocathode is a 10 mm diameter polished molybdenum disk coated with Cs_2Te with 5 mm diameter photosensitive area. It is illuminated by 263 μm wavelength laser light which is directed onto the photocathode by a 45° off-axis mirror located downstream of the RF coupler.

The photocathodes are coated at a separate facility on the Fermilab site, transported under vacuum to the photocathode transfer chamber mounted on the upstream end of the gun, and inserted into the upstream end of the gun via external manipulators, all under vacuum. Several photocathodes have already been prepared and their quantum efficiency measured to be ~10% when new. The photocathode preparation, transport, and transfer chambers were developed and built by D. Sertore at INFN Milano [2.3] and commissioned at Fermilab.

For emittance compensation the gun is surrounded by 2 solenoid magnets built by DanFysik, each powered by a 500 A power supply also built by DanFysik. Each magnet has a peak field of 0.28 T at 500 A. Normally the magnet currents are set so the field at the photocathode is 0 in order to minimize beam emittance, however the field can be set to > 1 kG at the photocathode for the production of angular-momentum dominated beams and flat beam production. Each solenoid can be moved transversally to center the magnetic field on the beam axis, and in addition the downstream solenoid can be moved longitudinally to further optimize the magnetic field shape. ASTRA [2.4] simulations indicate that transverse normalized emittances of 4 μm can be attained at a bunch charge of 3.2 nC, laser pulse length of 3.2 ps RMS, and peak gun electric field gradient of 40 MV/m. Stretching the laser pulse length will produce slightly smaller transverse beam emittance out of the gun, as will higher gun gradients.

PITZ fabricated a gun and coupler for ASTA, and Fermilab has fabricated 3 guns and couplers. One of these (gun and coupler) was shipped to KEK for beam studies, one is currently installed at ASTA awaiting commissioning, and two are spares. Figure 2.1 shows a cross-section drawing of the gun and adjacent vacuum components, and Figure 2.2 is a photograph of the gun installation at ASTA in August, 2012.

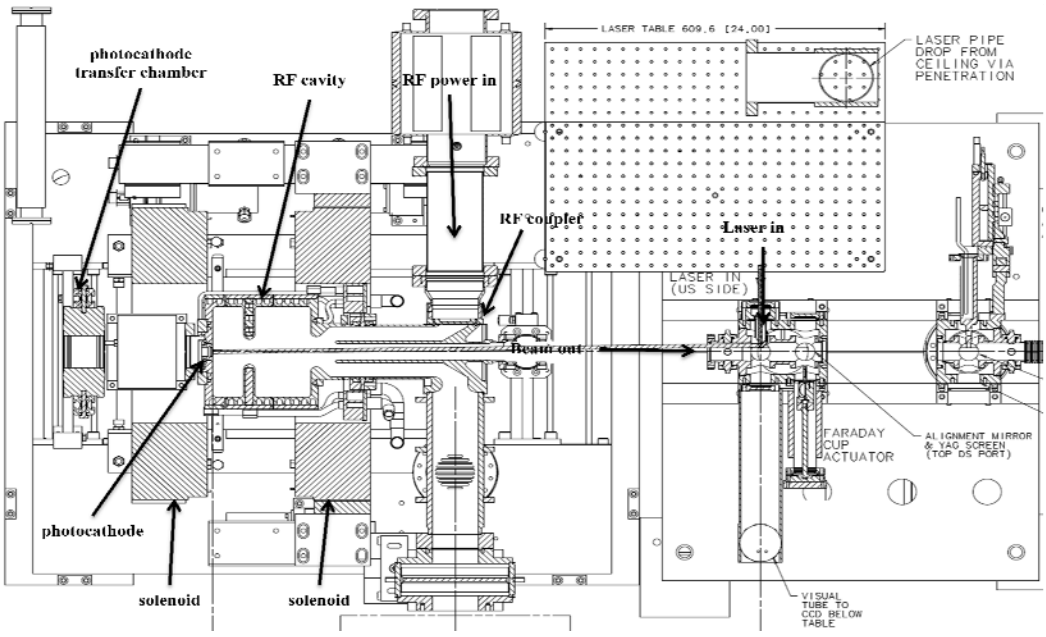

Figure 2.1: Cross section of gun, solenoids, transfer chamber, and downstream instrumentation.

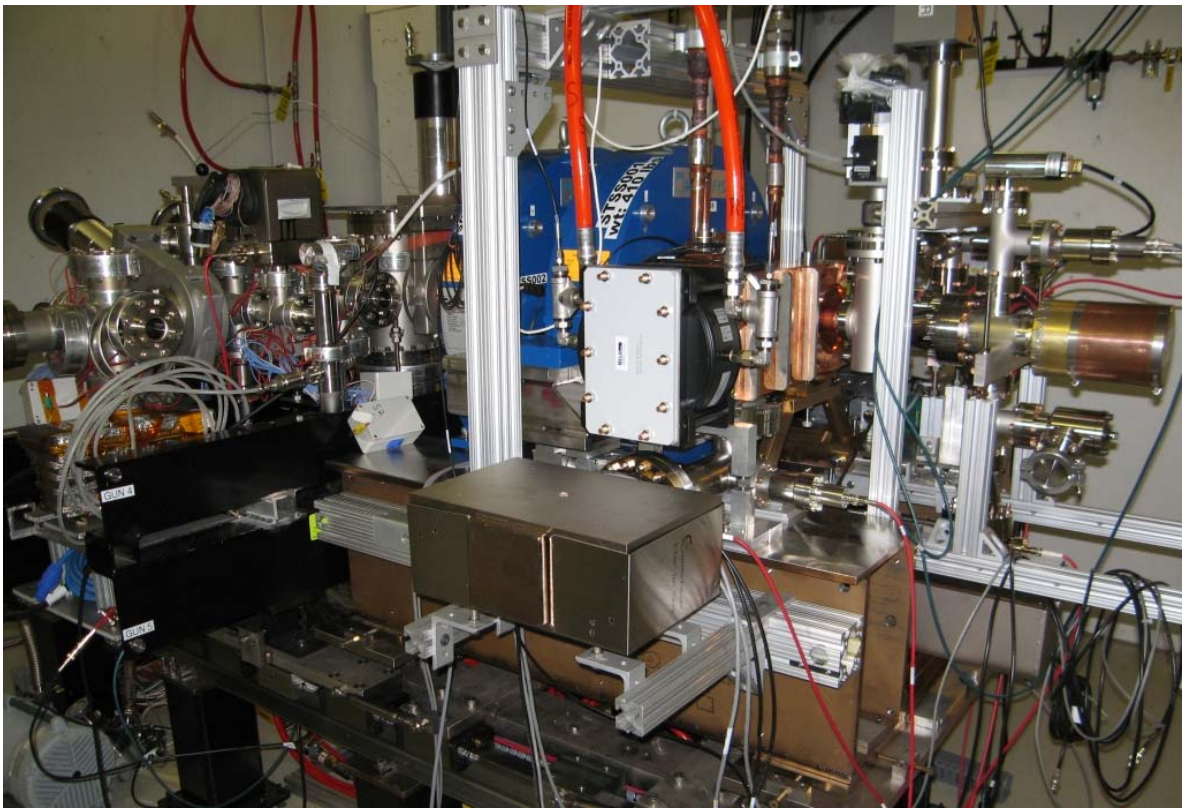

Figure 2.2: Photograph of the gun installation in the ASTA enclosure on August, 2012. Photocathode preparation chamber is to the left, and beam exits to the right. RF waveguide connection is towards the viewer (white blank-off). Solenoids are blue.

2.2 Initial performance

Five RF windows rated for 5 MW were purchased from Thales and separately conditioned at ASTA for both forward and reflected power using the CM1 klystron. The gun installation was completed in September 2012 and commissioning started in November 2012. Figure 2.3 is a schematic of the gun setup with relevant diagnostics and interlocked devices.

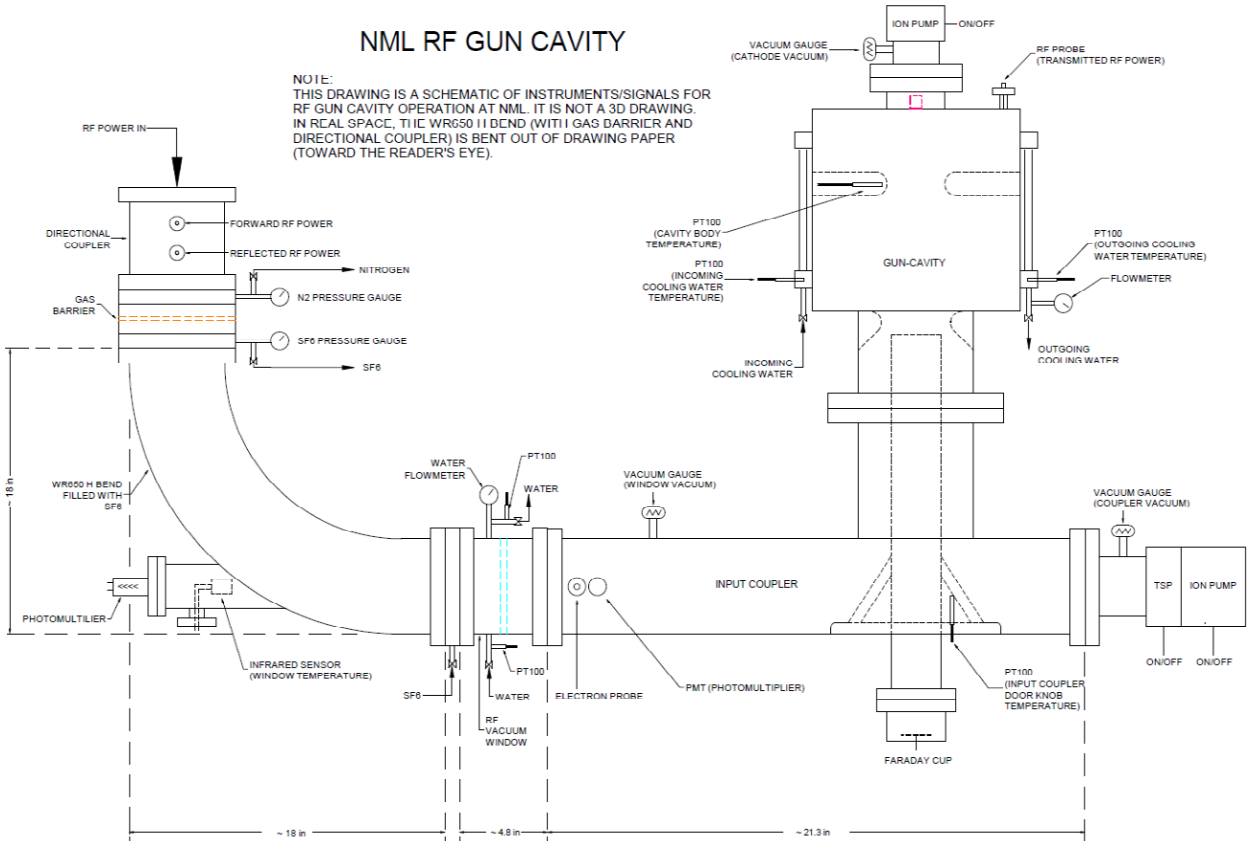

Figure 2.3: Gun schematic with interlocked and monitored devices during commissioning.

References

[2.1] M. Otevrel, *et al.*, "Conditioning of a New Gun at PITZ Equipped with an Upgraded RF Measurement System", WEPB05 in The Proceedings of FEL2010, Lund-Malmo, Sweden, Aug. 2010 (http://accelconf.web.cern.ch/accelconf/FEL2010/papers/wepb05.pdf)

[2.2] S. Lederer, *et al.*, "Conditioning of a New Gun Cavity Towards 60 MV/m at PITZ", TUPMN026 in The Proceedings of PAC07, Albuquerque, NM, June 2007 (http://pac07.org/proceedings/PAPERS/TUPMN026.PDF)

[2.3] D. Sertore, *et al.*, "Review of the Production Process of TTF and PITZ Photocathodes", MOPB009 in PAC05, Knoxville, TN, May 2005 (http://accelconf.web.cern.ch/accelconf/p05/PAPERS/MOPB009.PDF)

[2.4] K. Floettman, "ASTRA – A Space Charge Tracking Algorithm" (http://www.desy.de/~mpyflo/)

3 Photocathode laser

The photocathode laser system is housed in a dedicated, temperature and humidity controlled 8.7 m x 6.5 m room on the ASTA floor adjacent to the beamline enclosure. There are 3 optical tables inside the laser room – one table dedicated to the photocathode laser, one table intended for a high bandwidth Ti:Sa laser, and one table intended for future laser R&D. The uv laser light is transported into the tunnel enclosure via a vacuum pipe and 2 evacuated mirror boxes.

3.1 System design

The ASTA laser system is based on the design used for many years at the A0 photoinjector [3.1], with some notable improvements. One of the disadvantages of the A0 laser system design is the low efficiency of the gain medium, Nd:Glass, used in the amplifying structure. Coupled with the fact that the flash lamp used to pump the gain medium is relatively unstable, it is difficult to realize long pulse train operation as required in ASTA with such a system. In order to address this issue we are using Neodymium-doped yttrium–lithium fluoride (Nd:YLF) as the gain medium to replace the Nd:glass used in current A0 laser amplifier chain. Nd:YLF is a very efficient material that can be pumped by either flash lamp or diode laser. In addition the induced emission cross section is large enough to produce a single pass amplification up to 10. At the same time the flash lamp pump will be changed to a fiber coupled laser diode pump to get better stability and higher reliability. Using optical fiber to deliver the pump to the end-pumped active medium has several practical advantages:

- The pump beam at the end of the fiber has a high quality, central symmetrical profile.
- The radial size of the beam can be easily scaled up or scaled down with high quality optics.
- A fiber connection provides a simple and virtually lossless interface between the pump source and the active medium.
- Both the pump source and active medium can be changed simply by reconnecting the fiber between them.

In addition to the changing the amplifying chain we will also replace the solid state seed laser used at A0 with a fiber laser based seed system. Figure 3.1 is the designed flow chart of the entire photocathode laser system.

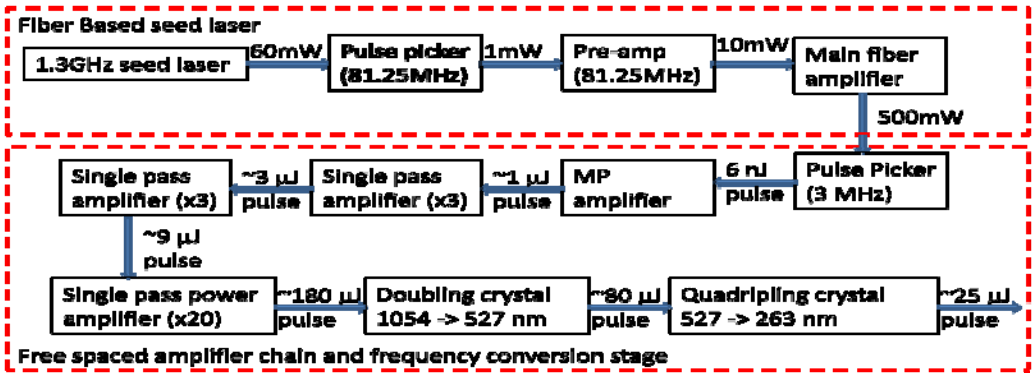

Figure 3.1: Design of the entire photocathode laser system. The expected power level at each stage is indicated.

3.2 Commissioning and preliminary tests

3.2.1 Fiber based seed laser

This system was designed and built at Calmar Laser Inc. Figure 3.2 is a photo of the entire system. The seed laser is an active mode locked Yb-fiber laser system centered at 1054 nm. The laser cavity consists of yttrbium doped fiber amplifier (YDFA), output coupler, electro-optics modulator, tunable filter and fibers that connect these devices together. A piezo stage is used to adjust the cavity length to achieve stable mode-locking. The pulse width is 3.2 ps RMS as measured with an auto-correlator, and the laser is locked to a 1.3 GHz signal from the low level RF master oscillator. The modulator bias voltage needs to be adjusted to a proper DC value to ensure proper mode-locking, but can drift over time. In order to accommodate this drift, a feedback system has been designed to adjust the modulator bias automatically to stay at the optimum value without tuning by the users. An RF spectrum is shown in Figure 3.3. The signal/noise ratio is well above 70 dB. Jitter studies using an Agilent E5052B signal source analyzer resolve a phase noise less than 200 fs integrated from 1 Hz to 10 MHz.

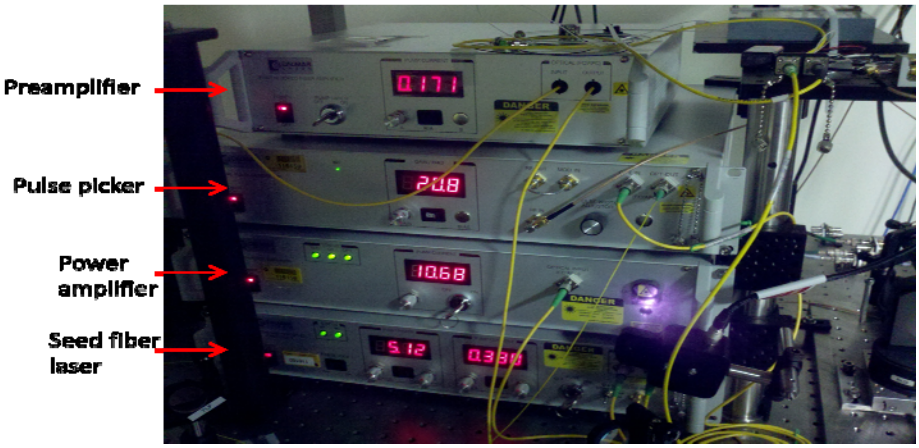

Figure 3.2: Fiber based seed laser system.

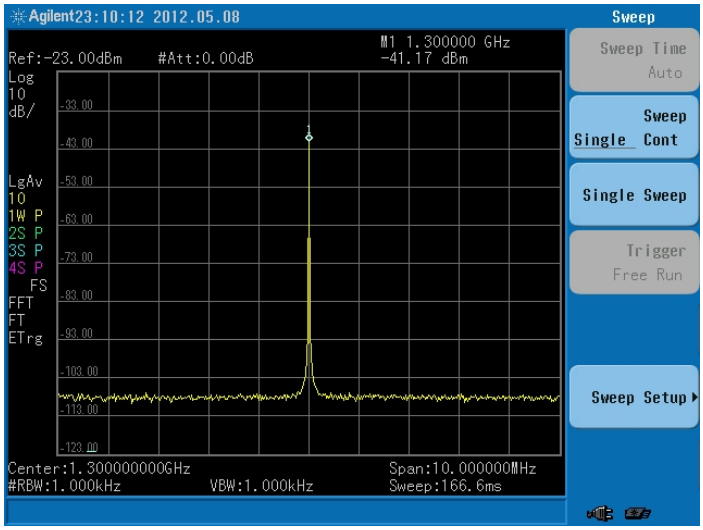

Figure 3.3: RF spectrum of the seed laser locked at 1.3 GHz

The fiber oscillator pulses are sent through a pulse picker (Calmar model EPG-01FML12), in which a 81.25 MHz pulse train is selected from the 1.3 GHz pulse input. The output is amplified in 2 stages to reach 5 nJ per pulse. Figure 3.4 shows a plot of the measured seed pulse phase over 1 hour after the entire system was warmed up for 10 hours. The standard deviation of the laser phase is 212 fs during this span without noticeable drift, which is much better compared to the same measurement with a similar setup on the GE-100 manufactured by Time-bandwidth Inc. or the Tsunami Laser system manufactured by Spectra-physics [3.2].

The output from the seed laser then goes through a second pulse picker unit (Con-optics) and is reduced to a 3 MHz train as required at ASTA. This pulse train can be up to 1 ms long. The extinguishing ratio through the pulse picker is more than 120:1, and the pulse-pulse amplitude fluctuations are less than 3%.

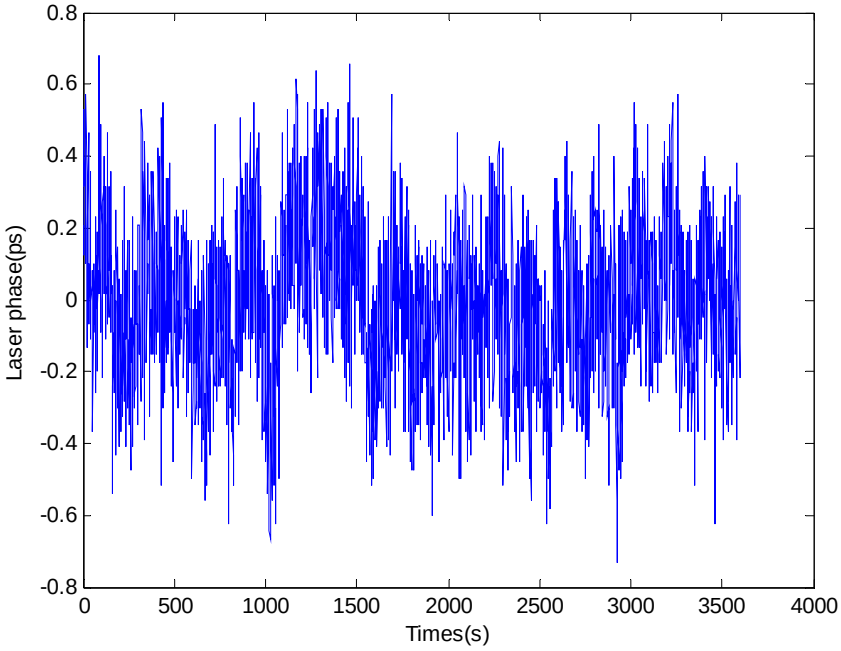

Figure 3.4: Seed laser phase measurement over 1 hour

3.2.2 Diode pumped multi-pass (MP) amplifier

For the demonstration of a free running end-pumped Nd:YLF laser we put the rod into a cavity with a length of 1.85 m as shown in Figure 3.5. The cavity used a flat output coupler with a reflectivity of 90% and an opposite reflector with a radius of curvature of 5 m. The lasing at 1054 nm is insured by the correct orientation of the Nd:YLF crystal using a previous single-pass small signal gain measurement. We also inserted a Brewster plate into the cavity which was used as the input and output port for future MP structures. The existence of the Brewster plate forces the cavity lasing only at 1054 nm because it acts as a polarizer inside the cavity. The wavelength of the output laser radiation was also confirmed by a commercial optical spectrum analyzer. At the maximum one-sided pumping energy of ~30 mJ, the free-running output was 3 mJ in the multi-longitudinal fundamental TEM_{00} mode, which is 10% of the pump energy delivered to the Nd:YLF rod surface. At the maximum two-sided pump energy of ~60 mJ, the

free-running output was 9 mJ for the TEM_{00} mode, which is about 15% of the energy delivered to the rod surface. In Figure 3.6 we have plotted the resonator output vs. the input energy for the two-sided pump case. The inset is the image of the TEM_{00} mode captured with a CCD camera. The highly symmetric image indicates a very good TEM_{00} mode.

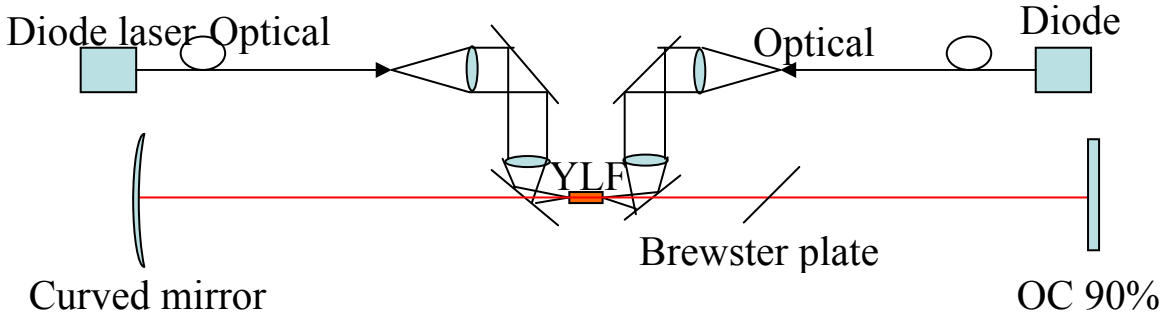

Figure 3.5: The end-pumped 1054 nm Nd:YLF laser resonator layout.

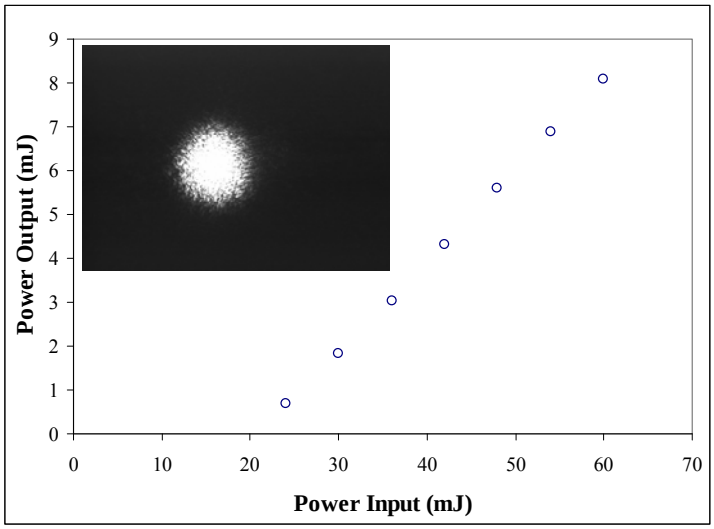

Figure 3.6: Measured output energy vs. the pump energy. The inset shows the spatial profile from the TEM_{00} mode captured with a CCD camera.

It's worth noting that we observed the good mode throughout the entire pump range without any transverse control inside the cavity. This could be explained by the fact that the end-pumped cross section is smaller than the fundamental mode, which will function as an automatic mode control inside the cavity. The optical to optical differential efficiency in our case is 15%. In order to realize MP, a Q-switch unit will be put in between the Brewster plate and the flat HR mirror. Initial tests of single pass operation with Q-switch unit yield a gain of more than 4.

We tested the MP operation at another lab before moving it to the ASTA laser room. These results are shown in Figure 3.7. The input of the 3 MHz pulse train is shown on the left side. The pulse energy at this point is about 1 nJ per pulse. The output of the pulse from MP cavity is shown on the right side of Figure 3.7. The output is very flat during the entire 1 ms long period. The energy at this point is above 2 μJ, so the total amplification is about 2000 times with 14

round trips. It's worth pointing out that in this configuration the pulse is very close to the saturation stage, which means our MP operation is actually a regeneration process.

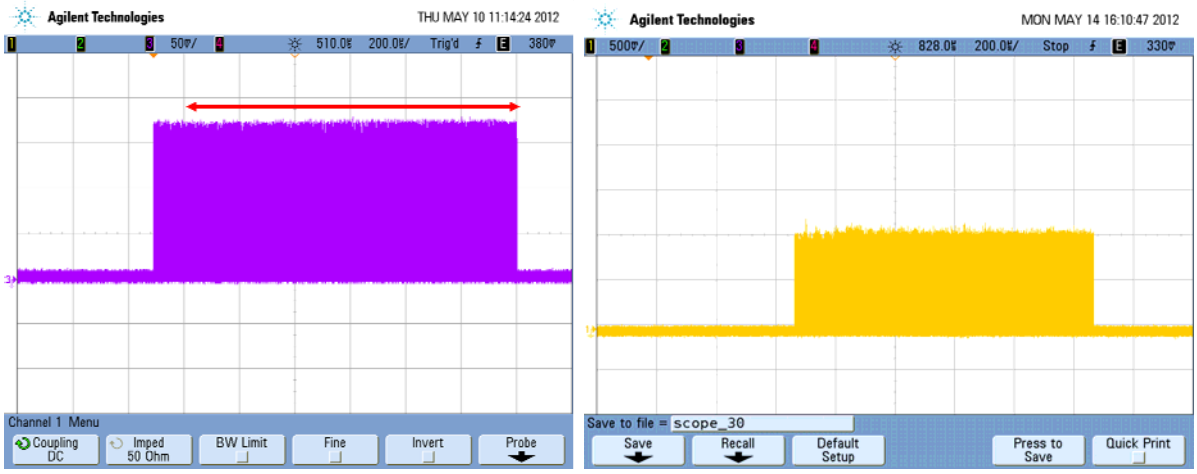

Figure 3.7: Oscilloscope image of the MP input (left side) and MP output (right side). The pulse energy is 1 nJ at the input and above 2 μJ after the MP cavity. The red arrow indicates a length of 1 ms.

3.2.3 Future development and additional laser systems

In the very near future we are planning to upgrade the entire amplifying chain with single pass or double pass amplification only, which will give us the possibility of running even higher repetition pulse trains. For example, a 6 MHz pulse train is desired for the proposed proof-of-principle experiment of an XUV FEL oscillator. We also have plans to develop a laser system for a proposed Laser Compton scattering experiment based on our current configuration.

Several other laser systems will also be installed and developed once the photocathode laser system is fully operational. A Ti:Sa laser system will be installed and used for proposed future electro-optic sampling and optical beam position monitor experiments. An Er-doped fiber laser will be commissioned to perform the proposed beam arrival monitor experiment. At the same time an optical parametric amplifier using both the Ti:Sa system and the current driver laser system will be developed to support proposed laser induced microbunching studies at ASTA.

References

[3.1] J. Li, *et al.*, Nucl. Instr. and Meth. A **564** (2006) p. 57.

[3.2] T. Maxwell, *et al.*, "Synchronization and Characterization of an Ultra-short Laser for Photoemission and Electron Beam Diagnostics Studies at an RF Photoinjector", FERMILAB-PUB-11-657-APC (2011) (http://lss.fnal.gov/archive/2011/pub/fermilab-pub-11-657-apc.pdf)

4 Beamlines

4.1 Low energy beamline layout

The injector beamline is shown in Figure 4.1. After a short instrumentation section, the electron gun is followed by two SRF cryomodules to accelerate beam to 50 MeV. Each of these cryomodules contains a 9-cell L-band cavity operating at 1.3 GHz, driven by a 300 KW klystron, and capable of average accelerating gradients of >22 MV/m [4.1]. These cavities will also be used to "chirp" the beam, *ie.*, generate a time-momentum correlation, in preparation for bunch compression in the chicane. Downstream of these cavities is space allotted for a future SRF 3.9 GHz cavity intended to be used for bunch linearization during bunch compression.

The SRF cavities are followed by a quadrupole doublet to control the beam size for the emittance measurement, 3 skew quads to generate flat beam, a matching section into the chicane, a 4-dipole chicane for bunch compression (R_{56} = -0.18 m), a matching section into the vertically downward-bending dipole to the low energy beam dump, and finally a matching section into the first 8-cavity cryomodule. The 22.5° dipole upstream of the dump will serve as the low energy spectrometer. There is beamline space allocated upstream of this dipole for the future installation of a 3.9 GHz deflecting mode cavity to be used for longitudinal phase space diagnostics. The 50 MeV beam dump will be capable of absorbing up to 400 W of beam power, which is 15% of the full ILC intensity [4.2]. In addition, there is a dogleg to deliver 50 MeV beam to a test beam area parallel to the 1st cryomodule. This test area is intended for AARD experiments and is currently under design. The beam dump in this line will be identical to the beam dump in the injector line.

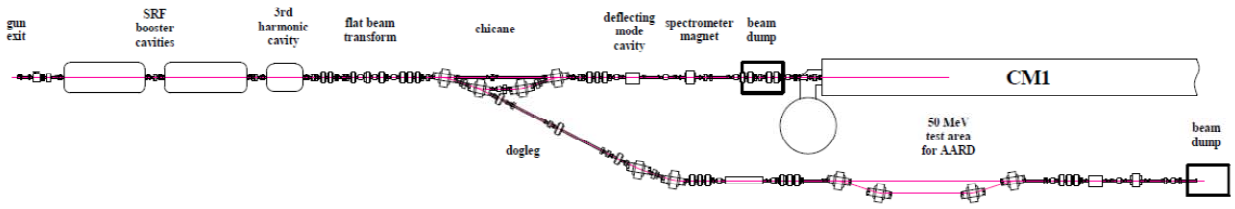

Figure 4.1: Injector layout.

4.2 High energy beamline layout

The beam will be initially transported from the cryomodule string to the first high energy spectrometer magnet by a 4-quadrupole matching section, a 4-quadrupole FODO lattice, and an additional 4 quadrupole matching section. This region of beamline is 45 m in length and is intended to house future AARD experiments, so it will be reconfigured from time to time to accommodate new experiments. The high energy beamlines downstream of this section are shown in Figure 4.2. There are 2 dispersion-cancelling doglegs which allow for two 10 m sections reserved for AARD experiments. The final 2 quads in the beamline are to be used to blow up the transverse beam size to avoid damage to the beam dump core. There is a 6" dia. hole through the beam dump to allow the passage of beam or FEL light to a possible future facility downstream of ASTA.

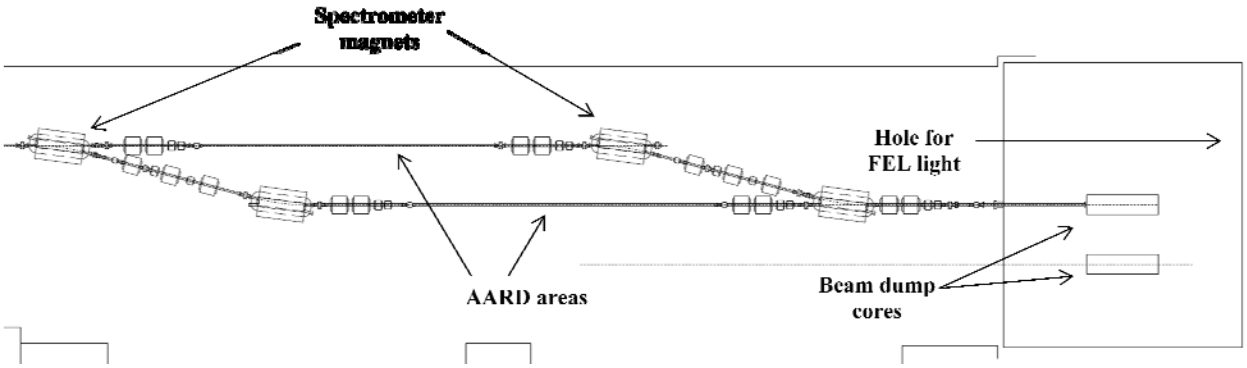

Figure 4.2: High energy beamline experimental area and beam dumps.

4.3 Magnets

There are 6 different types of magnets for ASTA (in addition to the gun solenoids): low energy correctors, quadrupoles, and dipoles; and high energy correctors, quadrupoles and dipoles. All magnets are bolted in 2 halves for possible removal or installation without breaking beampipe vacuum. All magnets can accommodate 2" O.D. vacuum pipe

4.3.1 Low energy dipole correctors

The low energy corrector magnets are air-cooled and were fabricated by Radiabeam Technologies, Inc. Each magnet has both horizontal and vertical corrector coils, and the magnet was designed to bolt around 3 3/8" conflat flanges. The maximum integrated field is 12.5 G-m at 7.6 A, which gives a beam kick of 7.5 mrad for 50 MeV beam. See Figure 4.3 for a magnet cross section. In addition, 3 smaller corrector magnets from the A0 photoinjector, of a similar design, will be used at the low energy end of the injector.

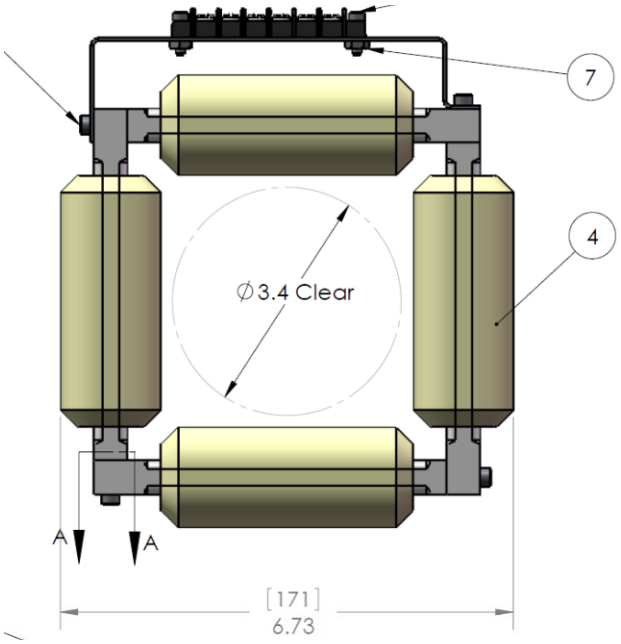

Figure 4.3: Low energy corrector dipole cross section.

4.3.2 Low energy quadrupoles

The low energy quadrupoles are air-cooled and were fabricated by Radiabeam Technologies, Inc. The maximum integrated field is 1.1 T at 9.0 A, which gives a focusing strength (K x L) of 6.6 for 50 MeV beam. The effective magnet length is 0.167 m. See Figure 4.4 for a cross section. In addition, 3 smaller quadrupoles from the A0 photoinjector, of a similar design, will be used in the injector chicane. Skew quadrupoles are identical and are simply mounted at 45° from normal quadrupoles.

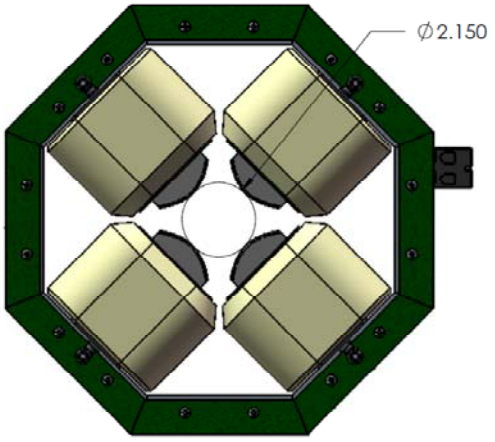

Figure 4.4: Low energy quadrupole cross section.

4.3.3 Low energy dipoles

The low energy dipoles are air-cooled and were fabricated by Everson Tesla Corp. The maximum integrated field is 665 G-m at 8.0 A, which gives a beam kick of 23.5 deg for 50 MeV beam. The effective magnet length is 0.300 m. See Figure 4.5 for a cross section. The clear aperture in the kick direction is >24 cm. The dipole will be rotated 90° about the beam axis to generate the 22.5° downward kick for the low energy beam dump line.

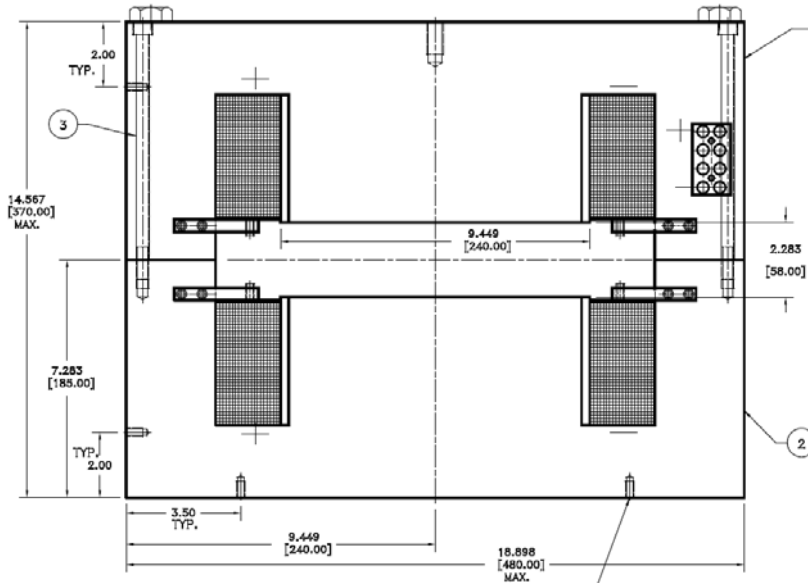

Figure 4.5: Low energy dipole cross section.

4.3.4 High energy dipole correctors

The high energy corrector magnets are air-cooled and were fabricated by Everson Tesla Corp. This magnet will serve as both horizontal and vertical corrector by rotating the magnet 90° about the beam axis for vertical correctors. The maximum integrated field is 200 G-m at 9.2 A, which gives a beam kick of 6.7 mrad for 900 MeV beam. See Figure 4.6 for a magnet cross section.

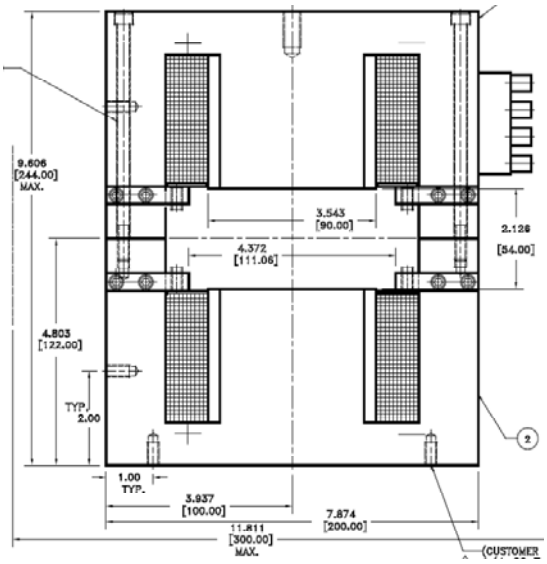

Figure 4.6: High energy corrector dipole cross section.

4.3.5 High energy quadrupoles

The high energy quadrupoles are water-cooled and were fabricated by Everson Tesla Corp. Water flow rate is 0.41 GPM (per magnet). The maximum integrated field is 8.3 T at 60 A, which gives a focusing strength (K x L) of 2.8 for 900 MeV beam. The effective magnet length is 0.417 m. See Figure 4.7 for a cross section.

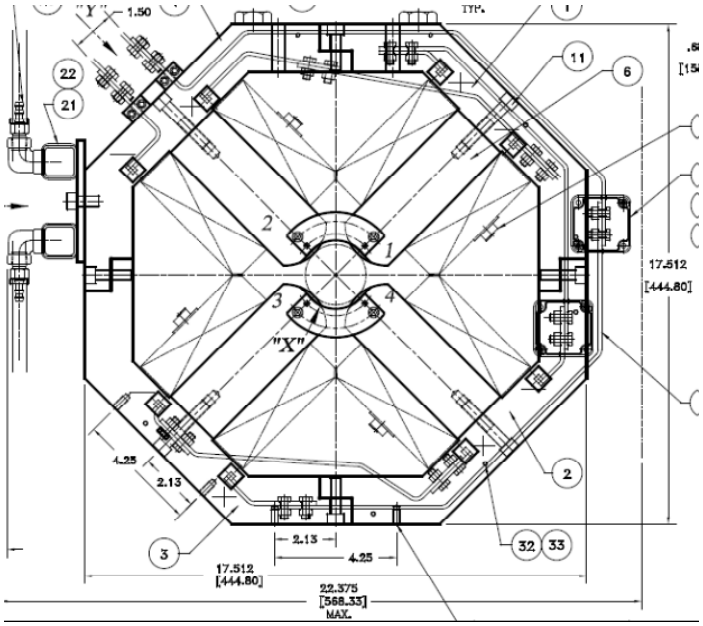

Figure 4.7: High energy quadrupole cross section.

4.3.6 High energy dipoles

The high energy dipoles are fabricated from spare MI dipole laminations and spare MI dipole conductor. The laminated magnet cores were stacked by Fermilab, and the magnet was wound and assembled by Everson Tesla Corp. These magnets are water-cooled and take 7.5 GPM (per magnet). The maximum integrated field is 1.33 T-m at 1000 A, which gives a beam kick of 26.1° for 900 MeV beam. Effective magnet length is 1.277 m. See Figure 4.8 for a cross section. The clear aperture in the kick direction is 27.3 cm.

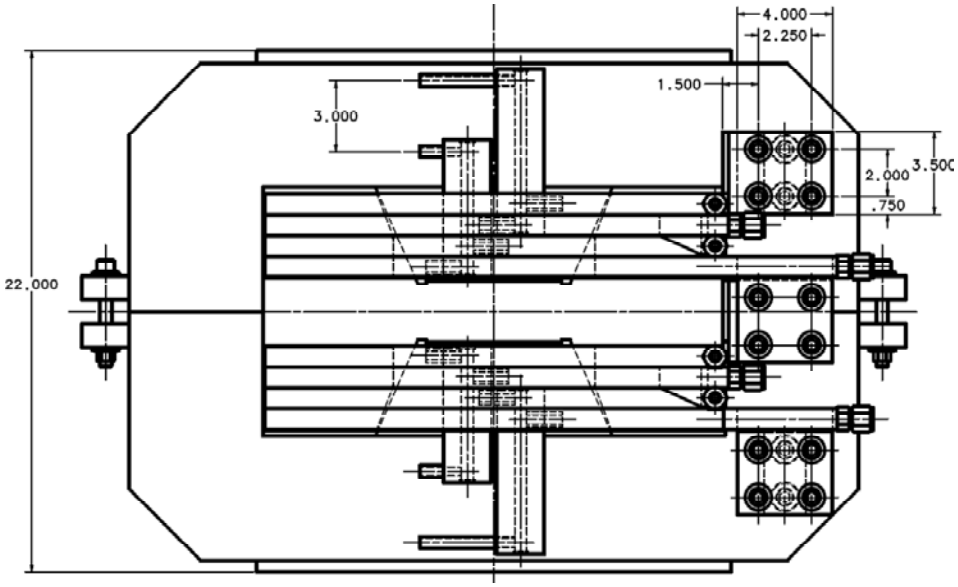

Figure 4.8: High energy dipole cross section.

4.3.7 Power supplies

Table 4.1 lists magnet power supply parameters. The 10 A and 60 A power supplies are similar in design to the standard FNAL Main Injector bulk power supplies and regulators [4.3].

Table 4.1: Magnet power supply parameters

associated magnet	LE corr.	LE dipole	LE quad.	HE corr.	HE dipole	HE quad.
# installed magnets	28	12	32	29	4	29
total # PS (+15% spares)	64	14	37	33	5	33
int. field max. [G-m] or [T]	12.5	640.0	1.1	200.0	13300.0	8.3
magnet inductance [mH]	38	2250	104	149	23	123
magnet resistance [ohms]	0.160	5.400	1.333	1.456	0.0116	0.317
magnet resistance (at max current) [ohms]	0.168	5.670	1.400	1.529	0.0122	0.333
Imax [A]	7.6	7.7	9.0	9.2	1000.0	60.0
Imax _full scale [A]	10.0	10.0	10.0	10.0	1000.0	60.0
polarity	bipolar	bipolar	bipolar	bipolar	unipolar	bipolar
Vmax (@ Imax DC) [V]	1.3	43.7	12.6	14.1	12.2	19.0
minimum bits required	12	16	16	12	16	16

regulation [%]	0.200	0.010	0.030	0.200	0.010	0.010
ripple [%]	0.0200	0.0010	0.0030	0.0200	0.0010	0.0010
bend at max. field spec. [mrad]	7.5 (50 MeV)			6.7 (900 MeV)		
bend at max. field spec. [deg]		22.6 (50 MeV)			26.1 (900 MeV)	
K x L at max. field spec.			6.6 (50 MeV)			2.8 (900 MeV)

4.4 Vacuum

The ASTA beamlines and beamline components are designed for a vacuum of <1.5E-8 Torr, except in the region of the RF gun which has more stringent vacuum requirements. All vacuum components downstream of the photocathode are fabricated, assembled, and installed as "particle-free" to avoid possible contamination of the SCRF cavities. Vacuum tube is made from electropolished 316L stainless steel and joined with conflat flanges. The warm vacuum tube is everywhere 2" O.D., except just upstream of the beam dumps where it is 3" O.D., and inside the dipole magnets, where large aperture is required and the vacuum pipe is custom made from aluminum with explosion bonded conflat flanges. Pneumatic, all-metal gate valves isolate the 50 MeV injector beamline into 8 vacuum sections: photocathode transfer chamber, electron gun, 9-way cross, CC1, CC1-CC2 interface, CC2, upstream of chicane, and downstream of chicane. Gate valves isolate the high energy beamlines into 3 vacuum sections. All cryomodules have internal cold gate valves and warm gate valves on either end. The cryomodule string has additional fast-acting warm gate valves (closing time = 15 msec) on either end. The vacuum pumping is done by a combination of conventional and noble diode ion pumps to balance good pumping speed with noble gas pumping capability. Vacuum levels are monitored with cold cathode and convection gauges in all vacuum sectors. Warm gate valves are not RF shielded, but most of the instrumentation and vacuum crosses have their ports RF shielded. All vacuum devices are interfaced to the ACNET controls system.

4.5 Diagnostics overview

There are four primary types of diagnostics in both the injector and the high energy beamlines: BPMs to measure beam position, profile monitors to measure beam size, resistive wall monitors to measure beam current (4 in the primary injector beamline), and loss monitors (~40 total) to measure beam losses and serve as the primary protection element in the machine protection system. The first three of these are described in more detail in chapter 7, and the last is described in detail in chapter 9.

Each BPM is a 4-button pickup measuring both horizontal and vertical beam position. The system will be capable of bunch-by-bunch measurements, and the anticipated accuracy is <25 μm. There will be 23 BPMs in the primary injector beamline.

The profile monitors are located in 6-port vacuum crosses and were fabricated by Radiabeam Technologies. A prototype was tested at the Fermilab A0 photoinjector [4.4] and a resolution of < 20 μm has been obtained. They each contain a Ce-doped 100 μm crystalline yttrium aluminum garnet (YAG) screen or a 100 μm crystalline lutetium-yttrium oxyorthosilicate

(LYSO) screen, a 1 μm Al screen for OTR production, and a target screen for calibration. The screens are at right angles to the beam and are followed by a 45° mirror to deflect optical light to an optical channel and a 5 megapixel camera.

In the injector beamline, transverse emittance will be measured by the "slits method" both upstream and downstream of the chicane. Beam energy will be measured by the 22.5° spectrometer magnet. Bunch length will be measured by streak camera and interferometer.

Immediately downstream of the electron gun is the "9-way cross" (see Fig. 2.1) which provides the following instrumentation and functionality:

- UV window and mirror to direct the photocathode laser to the photocathode
- insertable mirror for viewing the photocathode region, with viewport
- insertable YAG screen and calibration target for beam size measurement, with optical channel and camera
- insertable Faraday cup for beam intensity measurement (low intensity only)
- insertable dark current collimator, with intensity measurement
- resistive wall monitor for intensity measurement
- 2 BPMs for beam position measurement
- 2 corrector magnets for steering correction (both dimensions)
- vacuum pumping and monitoring

Diagnostics in the high energy beamlines are identical to diagnostics in the injector beamline. There will be 27 BPMs, 9 profile monitors, 2 resistive wall monitors, and ~20 loss monitors in the initial high energy beamline configuration. The "quad scan" method will be used for transverse emittance measurements, and energy measurements can be made at two of the 15° dipole spectrometer magnets.

4.6 Beam dumps

4.6.1 Low energy beam dump

Figure 4.9 shows the location of the low energy beam dump as it will be configured at ASTA. It is situated at the end of the 22.5° downward-pointing beam dump line, underneath the 50 MeV injection line, approximately 2 m in front of the 1st cryomodule. As shown in Figure 4.10, the absorber core consists of a wedged stack of graphite disks (the wedge configuration spreads out the energy deposition), surrounded by a water cooled aluminum jacket, surrounded by a steel sleeve, all embedded in a concrete block. A dedicated, closed-loop, radioactive cooling water skid (see chapter 13) will provide the cooling water to this beam dump plus a future identical beam dump situated at the end of the 50 MeV AARD beamline.

A full energy deposition, thermal, stress, radiation damage, and lifetime analysis has been done on this beam dump design [4.2] using MARS and Finite Element Analyses with ANSYS. Based on these calculations, the beam intensity to the low energy dump will be administratively limited to 1.00E13 electrons/pulse (15% of full ILC intensity). This is 375 W average at 5 Hz and 50 MeV. This limit is imposed due to the instantaneous thermal stress in the graphite caused by high local energy deposition by the very small beam. Unlike the high energy dump, there is not enough space available in front of the low energy dump to adequately defocus the beam or fast

sweep the beam on the absorber core. The beam will be slow swept (pulse-to-pulse) to spread the energy deposition.

The beam dump vacuum windows will consist of a 7 mm thick graphite disk sandwiched between two 1 mm thick TZM (titanium, zirconium, molybdenum alloy) disks.

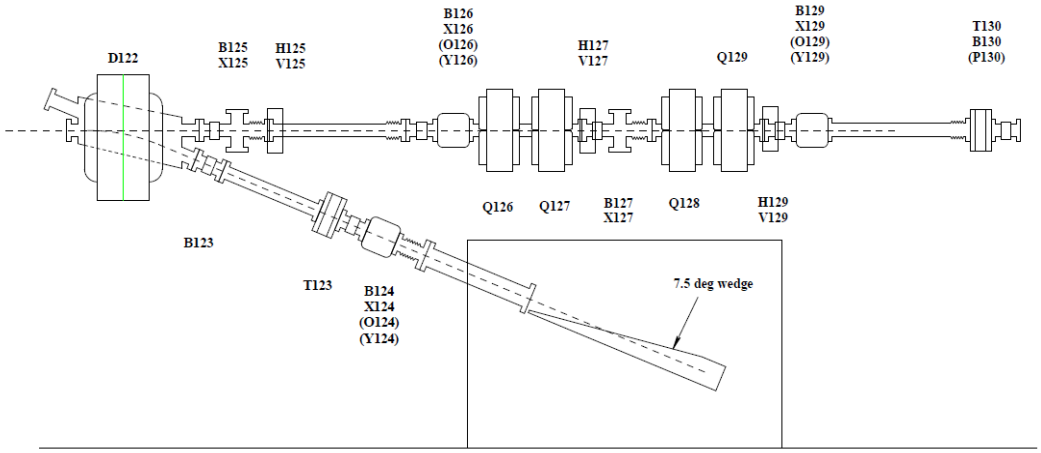

Figure 4.9: Low energy beam dump location.

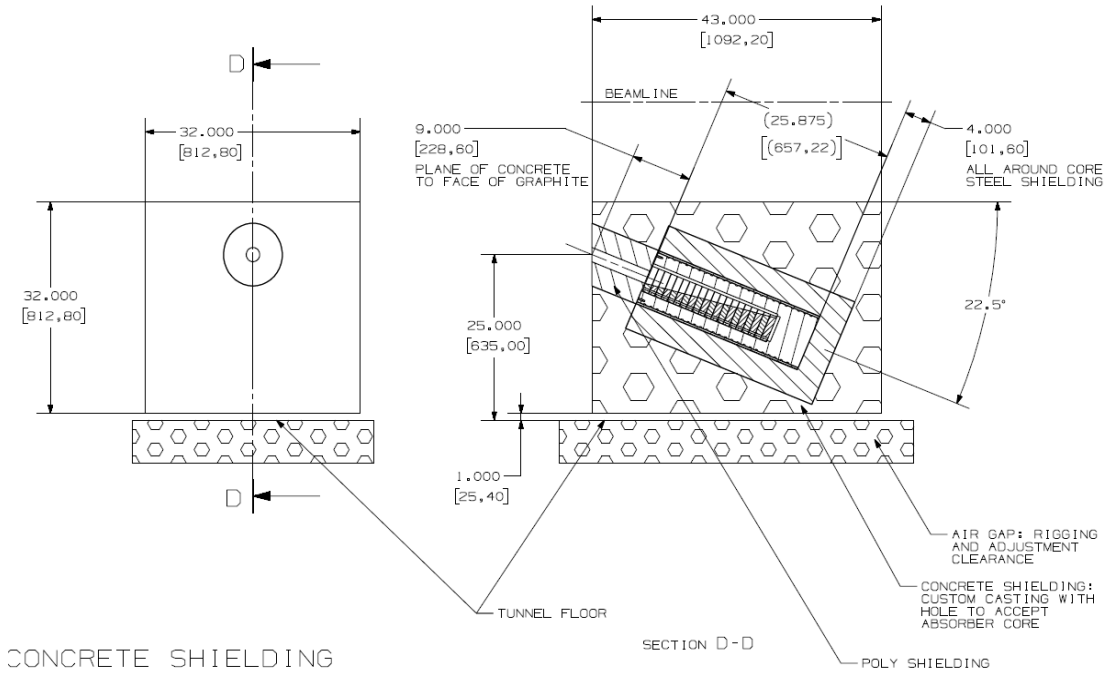

Figure 4.10: Low energy beam dump core materials.

4.6.2 High energy beam dump

The high energy beam dump is located in an alcove at the end of the high energy tunnel (see Fig. 4.2). This alcove opens to a hatch at ground level just downstream of the electrical service building, through which the concrete shielding blocks were stacked. The dump consists of two

absorber cores each surrounded by 1.5 m thickness of steel, all encased in a 6.1 m x 6.2 m x 7.3 m stack of concrete. As shown in Figure 4.11, the absorber core consists of a stack of graphite disks, surrounded by a water cooled aluminum jacket, and backed by a copper plug. A dedicated, closed-loop, radioactive cooling water skid (see chapter 13) will provide the cooling water to the two high energy beam absorbers in series. In addition, the entire dump core is encased in an inert gas (argon) to reduce oxidation of the graphite under the elevated temperature conditions.

A full energy deposition, thermal, stress, radiation damage, and lifetime analysis has been done on this beam dump design [4.5] using MARS and Finite Element Analyses with ANSYS. Based on these calculations, the beam dumps are designed to handle 80 KW of average beam power at energies up to 1500 MeV (full ILC intensity). The beam will be defocused by the final two quads in the beamline to a transverse spot size > 3 mm RMS in order to reduce the instantaneous peak energy deposition. In addition, the beam will be slow swept (pulse-to-pulse) by two corrector magnets at the end of the beamline to spread the damage potential throughout the graphite absorber.

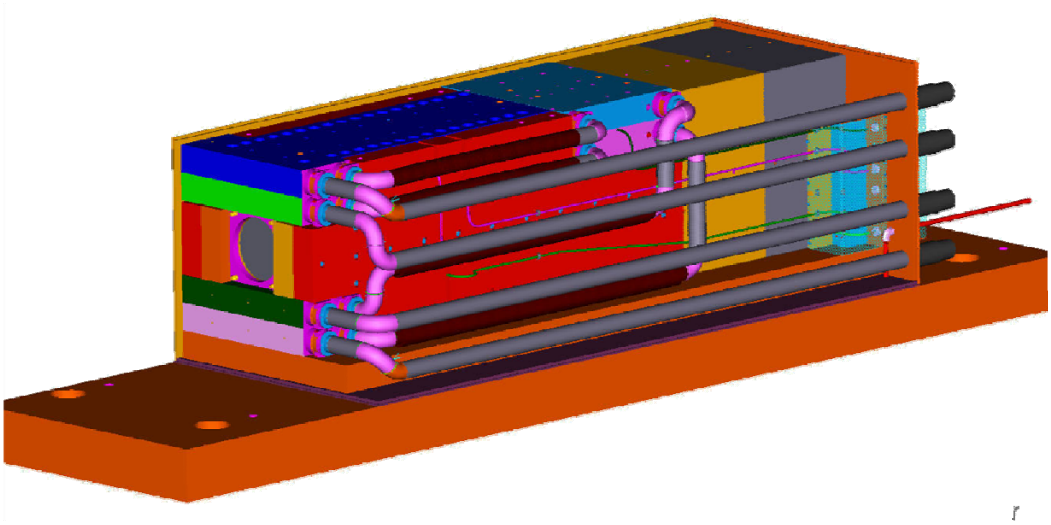

Figure 4.11: High energy beam absorber.

References

[4.1] J. Branlard, *et al.*, "Capture Cavity II Results at FNAL", WEPMN092 in PAC07, Albuquerque, NM, June 2007 (http://pac07.org/proceedings/PAPERS/WEPMN092.PDF)

[4.2] C. Baffes, "ASTA Low Energy Beam Dump Thermal Analysis", Fermilab Beams-Doc-4063, Feb. 2012 (https://beamdocs.fnal.gov/AD-public/DocDB/ShowDocument?docid=4063)

[4.3] L. Bartelson, *et al.*, "Four quadrant DC to DC Switching Supply for the Main Injector" in PAC97, Vancouver, BC, Canada, May 1997 (http://accelconf.web.cern.ch/accelconf/pac97/papers/pdf/5P007.PDF)

[4.4] A. Lumpkin, *et al.*, "Initial Beam-profiling Tests with the NML Prototype Station at the Fermilab A0 Photoinjector", MOP219 in NA-PAC11, New York, NY, Dec. 2011 (http://accelconf.web.cern.ch/AccelConf/PAC2011/papers/mop219.pdf)

[4.5] C. Baffes, "NML High Energy Beam Absorbers and Dump: Overview Talk", Fermilab Beams-Doc-3928, Aug. 2011 (http://beamdocs.fnal.gov/AD-public/DocDB/ShowDocument?docid=3928)

5 Cryomodules

5.1 Description

Two distinct cryomodule types are envisioned for ASTA consistent with those found in similar facilities worldwide. For the front end/low energy section a tandem of so-called "Capture Cavities" are found between the electron gun and the accelerating section. Multi-cavity cryomodules of the "Tesla" design are to serve as the main accelerating components. Regardless of Cryomodule type, all cavities are of a similar design:

- Fabricated of high purity (RRR>300) Niobium sheets
- 9-cell construction (Fig. 5.1)
- Length = 1.038 meter
- Resonant frequency = 1300 Mhz
- Nominal operating temperature = 2°K (23 Torr)
- Individual cavity welded into its own Titanium helium vessel (Fig. 5.2)
- "Slow" tuner
- Higher Order Mode damping accomplished by means of so-called "Formteil" antennae at each end of cavity
- Input couplers are of the waveguide to antenna design

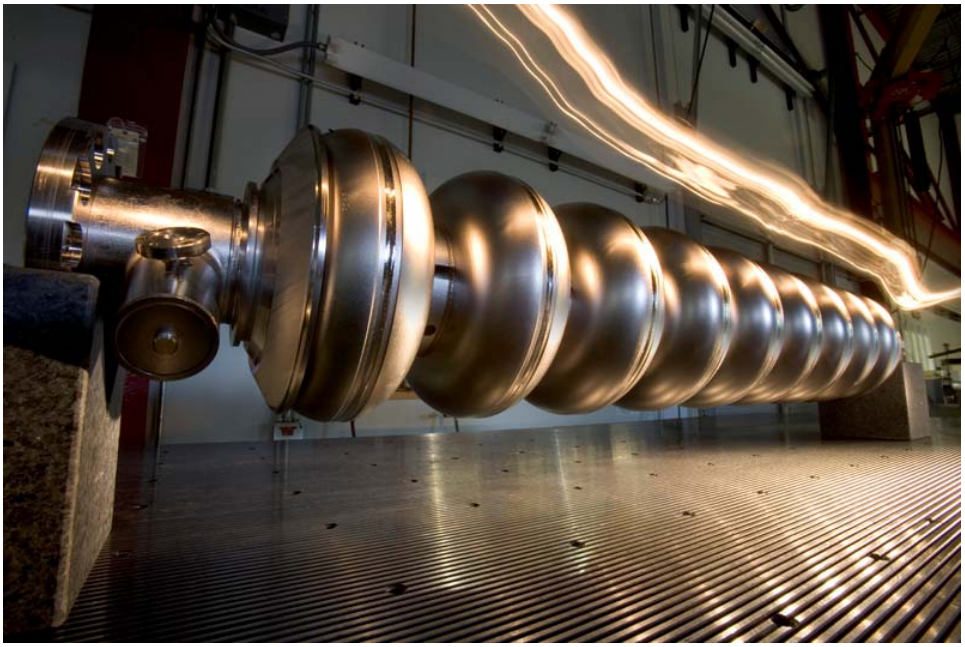

Figure 5.1: Bare Tesla style SRF Cavity

Figure 5.2: Dressed SRF Cavity welded into a Helium vessel

As is typical of Tesla style cryomodules the cavity vacuum is a closed loop system while the insulating vacuum is separate and partially integrated with the cryogenic system. Vacuum for the warm sections of the input couplers is also distinct for each cryomodule. In addition to the insulating vacuum space, thermal isolation from the outside is provided by thermal shields/intercepts at both 80°K and 5°K as well as insulating blankets. Common instrumentation is employed on the couplers – arc detection by means of photomultiplier tubes mounted to optical windows, field emission probes, and thermometry near the vacuum windows. These are all interlocked to limit the input power or shut off the RF system under predetermined fault conditions.

5.1.1 Capture cavities 1 & 2 (CC1, CC2)

The capture cavities are single 9-cell cavities in their own cryomodules. Both are based on an early Tesla/CEA Saclay design of SRF modules. The Capture Cavities to be placed into service at ASTA have been in previous service at Fermilab and elsewhere [1] [2] [3].

CC1 (Fig. 5.3) was the accelerating cavity used at the A0 Photoinjector for many years providing an average accelerating gradient of 14 MV/m. With the decommissioning of A0 in 2011, CC1 was removed and is in the process of being upgraded. While the vacuum shell is unchanged, a newer cavity, capable of generating >25 MV/m, is being installed. This new cavity will be outfitted with a blade-style tuner as opposed to the end-lever style one previously employed and which was largely non-functional while at A0 due to a shorted motor. As part of the upgrade the motor will also be replaced.

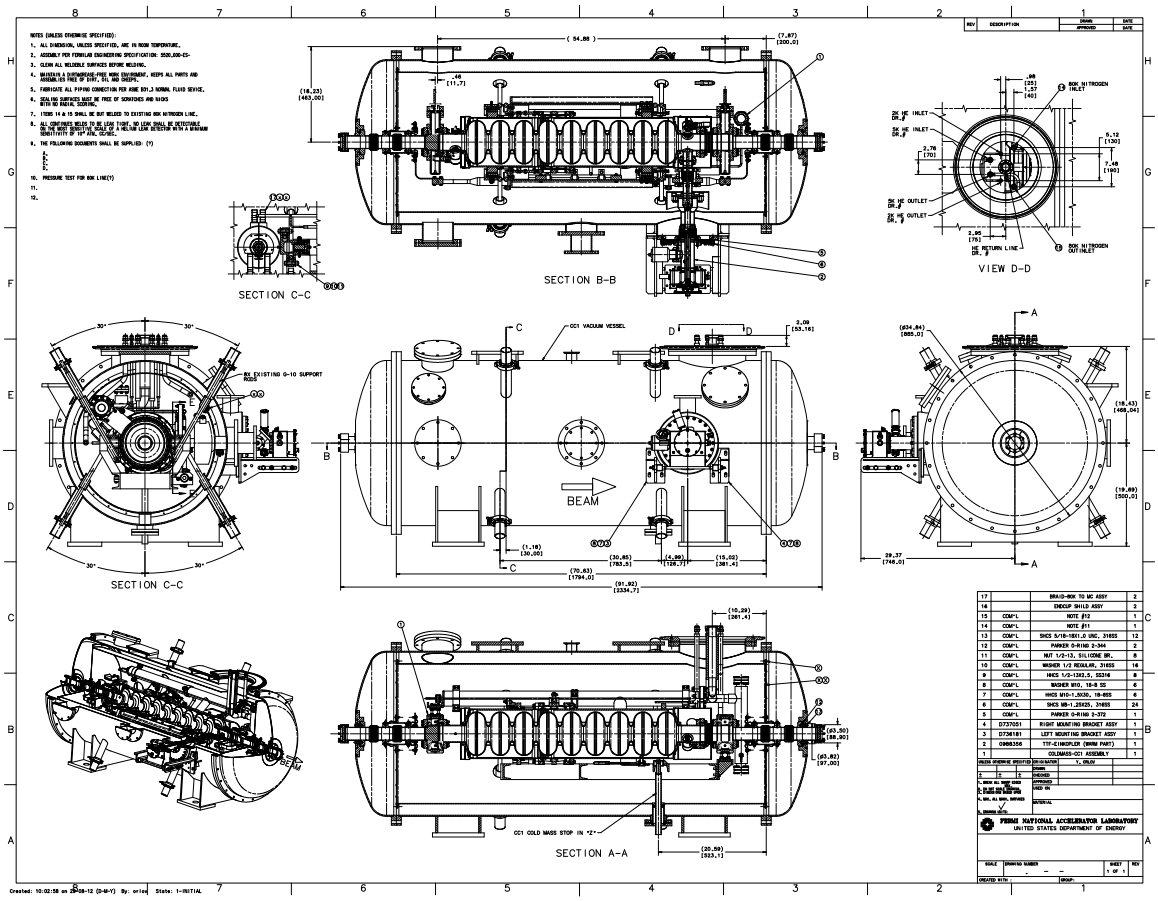

Figure 5.3: Capture Cavity Assembly Drawings

CC2 arrived at Fermilab as subassemblies from the DESY laboratory in Germany. They were assembled into a cryomodule and installed at the Meson Detector Building to provide Fermilab with a test bed to master SRF assembly and operation techniques. While at Meson Detector Building it achieved a peak gradient of 27 MV/m, but also suffered performance issues owing to excessive microphonics and a faulty input coupler. These shortcomings led to its removal and refurbishment. Following successful re-commissioning it was moved to ASTA (Fig. 5.4) to act as a heat load for commissioning the cryogenics plant serving at ASTA. At ASTA CC2 has been successfully operated up to 24 MV/m.

Both capture cavities are powered independently with their own Low Level RF controllers, separate 300 KW klystrons, and independent interlock/protection systems.

Figure 5.4: CC2 installed in the ASTA Enclosure. Electron gun is in background.

5.1.2 Multi-cavity cryomodules (CM1, CM2, CM3, …)

The remaining cryomodules, the first of which was CM1, are of a Tesla Type III+ design (Fig. 5.5) consisting of eight 9-cell cavities in a single cryomodule [5.4]. Each cavity has its own input coupler. In normal operation the entire 8-cavity string is driven via a single klystron by means of a waveguide distribution system provided by SLAC. The High Level RF and distribution system are described elsewhere.

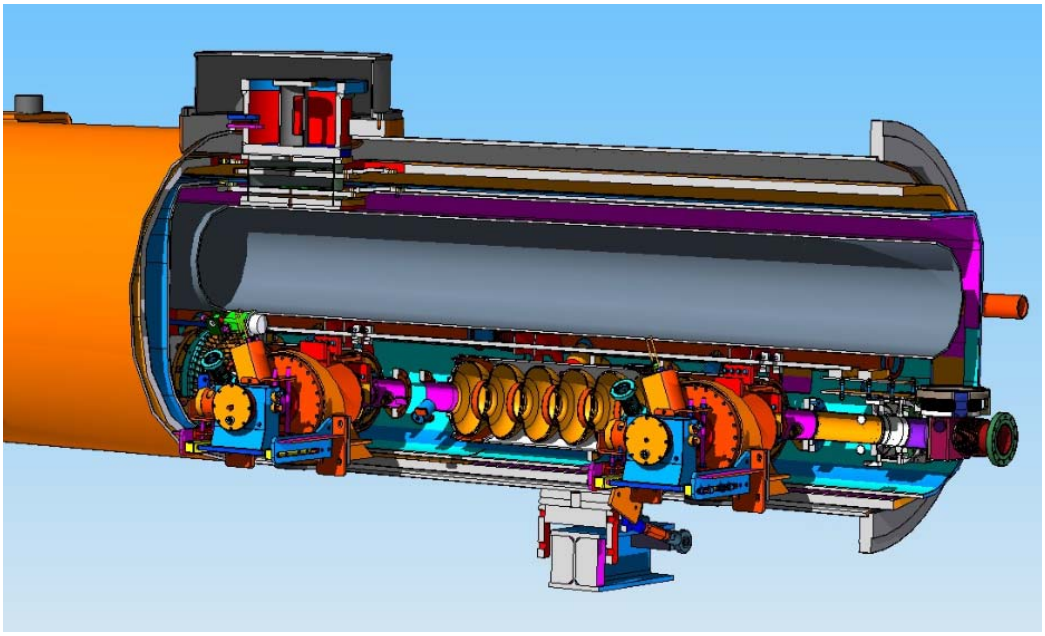

Figure 5.5: Cutaway view of a section of a TTF Cryomodule

The cavities comprising CM1 were provided by DESY where they were processed and tested individually in both "bare" (vertical) and "dressed" (horizontal) configurations. "Slow" and "fast" piezo-electric tuners are integrated into the cavity helium vessels. Slow tuners allow one to slowly/coarsely adjust the resonant frequency and are mostly used to put the cavities on resonance following cooldown or to compensate for long-term changes in conditions as well as frequency variations resulting from large changes in power. Their tuning range is of order hundreds of KHz with a resolution of a few Hz. Slow tuners are of a mechanical design which compress or stretch the "dressed" cavity. Fast tuners are integrated to the slow tuner body and are capable of a fast time response i.e. within the RF pulse albeit with a smaller tuning range than the slow tuners. The motion-active component is a piezoelectric device attached to the slow tuner body and is chiefly used to impart corrective forces in response to Lorentz Force Detuning.

Cavities are assembled into a string under clean room conditions and then integrated into the full cold mass assembly which is inserted into the outer vacuum vessel (Figs. 5.6, 5.7). The cavity string is mounted to a 300 mm diameter Gaseous Helium Return Pipe which provides the mechanical anchor and stability for the string. Cryomodule design and assembly is fully described elsewhere.

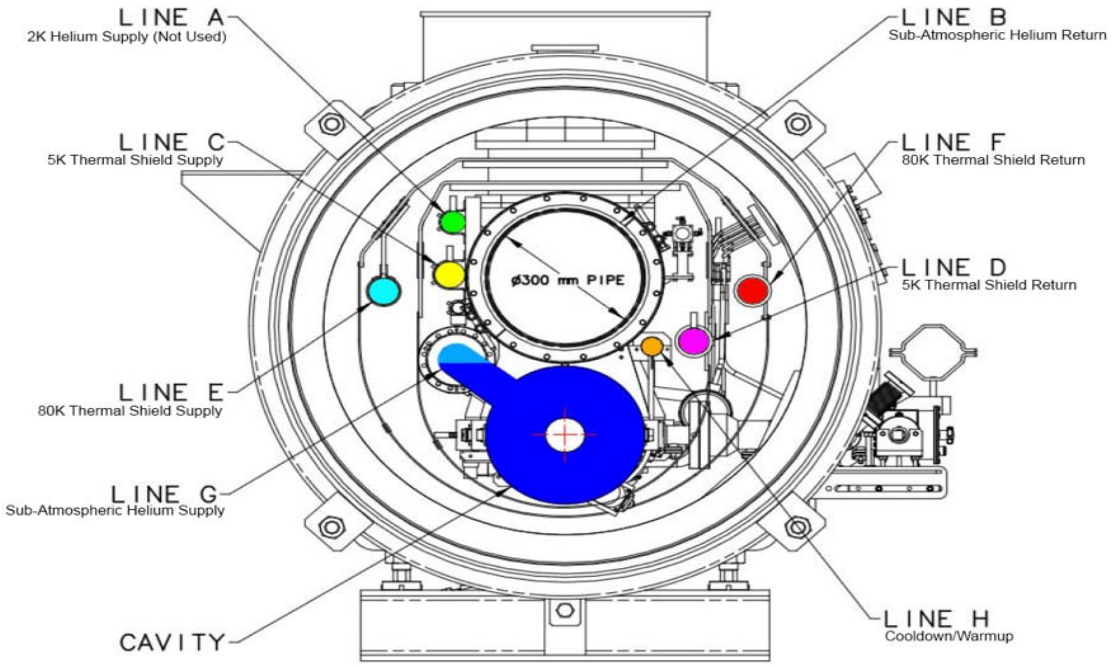

Figure 1. CM-1 Cross-Section (Looking Downstream from Feed Cap).

Figure 5.6: Cryomodule cross-section

Cryomodule installation is a weeks-long process to make the necessary vacuum, cryogenic, and instrumentation connections. Cryomodules are transported with the cavities vacuum sealed to prevent particulate contamination, hence all vacuum joints are made in cleanroom conditions to prevent the introduction and migration of any particulates which could adversely affect performance. Upon installation, the outer (warm) end of the input couplers must be attached,

also under clean room conditions. All vacuum and cryogenic connections are certified leak tight to 10^{-9} or better. Alignment requirements stipulate setting the device to 250 μm or better in all three planes.

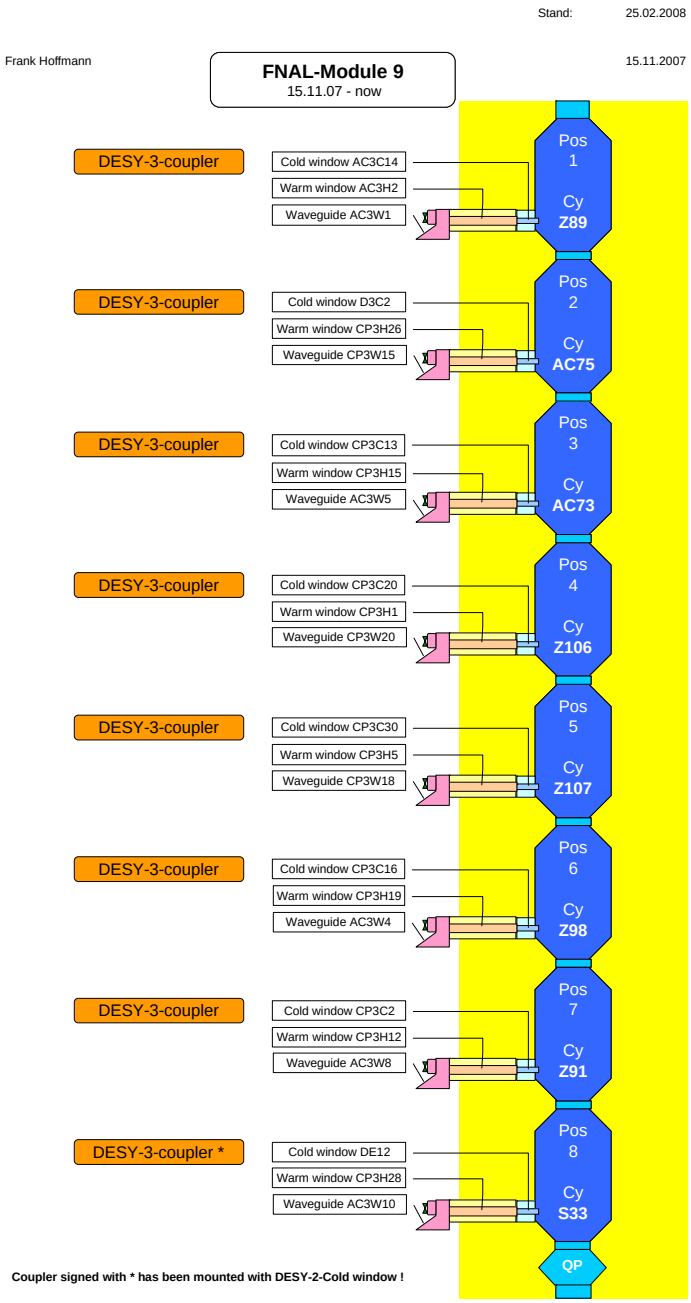

Figure 5.7: Cavity Layout for CM1

To date, CM1 has been installed and successfully operated in ASTA. This work is described in the following section. RFCA002, aka CM2 was briefly installed, but is now undergoing remediation for a vacuum leak on the 2ϕ helium circuit discovered during installation. All of the cavities comprising CM2 were manufactured by industry and tested either at Jefferson Lab or Fermilab. Based on these tests, there is good confidence that CM2's cavities will meet or exceed an average peak gradient of 31 MV/m (Fig 5.8).

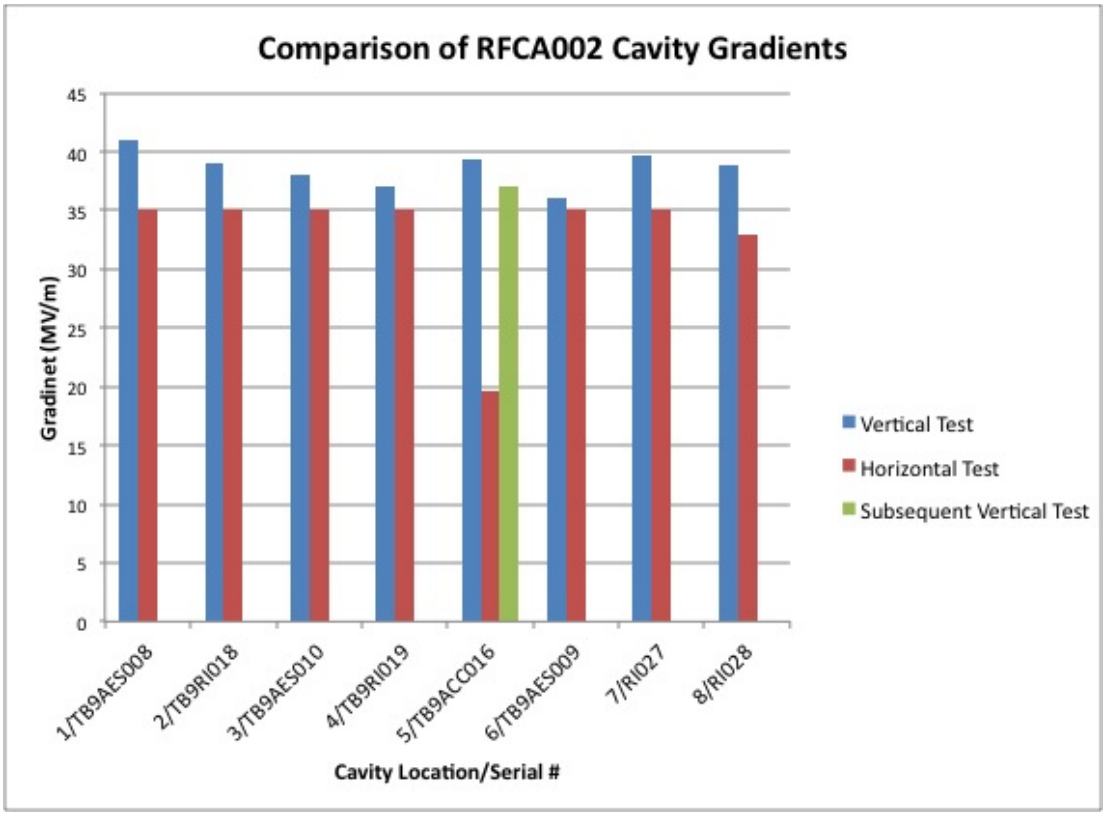

Figure 5.8: RFCA002 cavities test performance. For horizontal tests, an administrative upper limit of 35 MV/m was imposed. TB9ACC016 suffered from copper flaking in the coupler region during the horizontal test and was subsequently reprocessed and retested in the vertical test stand.

5.2 Initial performance

The first TESLA Type III+ 8-cavity cryomodule, CM1, was installed and operated in ASTA for approximately 15 months ending in March 2012. CM1 came to Fermilab as a "kit" and was assembled at Fermilab by the technical staff here with assistance from colleagues from DESY and LASA/INFN, Milano. Commissioning and testing followed the standard protocol developed worldwide for bringing cryomodules into full operation [5.5] [5.6] [5.7]. The steps include:

- RF Cable Calibration
- Technical Sensor/Interlock Check
- RF/Waveguide Check
- Warm Coupler Conditioning (off resonance)

- Cooldown to 2°K
- Frequency spectra measurements
- Cavity Tuning to 1.300 GHz via motorized slow tuner
- Q_L adjustment to 3.0E6
- LLRF calibrations
- Cold Coupler Conditioning (on resonance)
- Performance Evaluation including
    - Maximum gradient
    - Dynamic Heat Load (Q_0 vs. E_{ACC})
    - Dark Current and Field Emission (X-rays vs. E_{ACC})

CM1 was installed into its final position and aligned in January 2010 and final RF, cryogenics and vacuum connections were made thereafter. Warm off-resonance conditioning was performed with a single cavity at a time connected to the output of the 5 MW klystron and took anywhere from 2 weeks for the first cavity to 4 days to complete. Off resonance implies that the input RF was fully reflected back towards the load and no RF was directed into the cavity. The conditioning itself entails applying successively higher amounts of RF power in successively longer pulsed widths beginning with a 20 μs long pulse and eventually the full 1.3 ms pulse with peak powers in excess of 1 MW. An automated sequence was implemented which controlled the power and pulse width in a prescribed manner but responded to faults sensed by instrumentation monitoring excessive arcing, field emission, and vacuum.

Once all eight couplers were conditioned final vacuum work was completed leading to initiation of cooldown to 2°K. In slightly more than 2 days the module was cooled from room temperature to 4°K. The final cool-down to 2°K (23 Torr) required just 2-1/2 hours. CM1 first reached operating temperature on 22 November 2010.

Continuing with the sequence of commissioning steps, each cavity was then powered on resonance to complete coupler conditioning and determine cavity performance limitations. Again each cavity was powered singly. All cavities were characterized by June 11 as shown in Table 5.1 and Figure 5.9.

Table 5.1: CM1 individual cavity performance characteristics.

Cavity	**Peak E_{acc} (MV/m)**	**Estimated maximum Q_0 (E09)**	**Limitation/Comments**
1/Z89	20.2	11	'soft' quench/heat load
2/AC75	22.5	12	Quench
3/AC73	23.2	0.43	'soft' quench/heat load
4/Z106	24*	2.3	*RF-limited
5/Z107	28.2	39	Quench

6/Z98	24.5	5.1	Quench
7/Z91	22.3	4.7	'soft' quench/heat load
8/S33	25	18	Resonant frequency at 1300.240 MHz; tuner motor malfunction

Three cavities exhibited unexpectedly high heat loads as evidenced by cryogenic activity and a drop in the Q_L at relatively low gradient (<20 MV/m). It was found that the onset of the Q drop could be delayed by shortening the flattop pulse length from the nominal 620 μs to 100 μs. No source of this excessive heating has been definitely identified. Such behavior is not uncommon elsewhere and with CM1 now removed, plans are being made to disassemble the cavity string and re-evaluate these under-performing components one at a time in Fermilab's Horizontal Test Stand. Additionally the slow tuner on cavity #8 ceased functioning after approximately 20 minutes of cold operation leaving the cavity +240 kHz from the nominal 1.3 GHz resonant frequency. On-resonance tests were performed by adjusting the LLRF master oscillator but this failure did preclude any inclusion of Cavity #8 in full module tests.

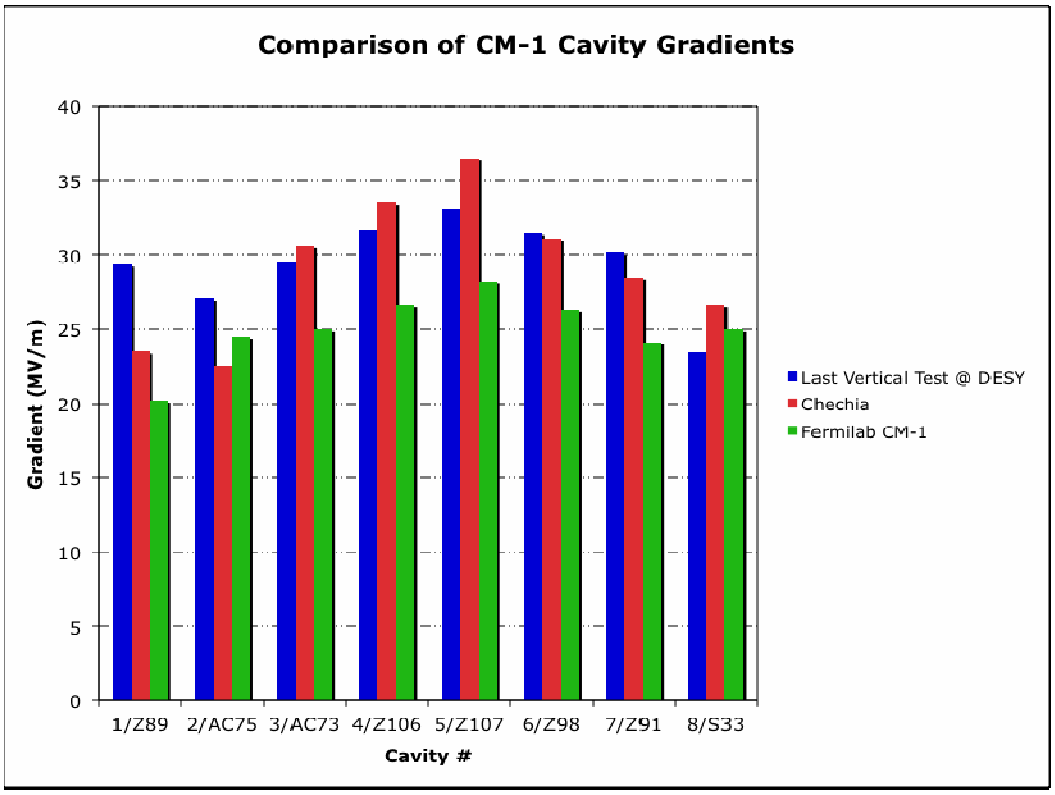

Figure 5.9: Comparison of cavity peak gradients – DESY single cavity vertical (blue), horizontal (Chechia) (red), and the complete CM1 at Fermilab (green).

Full module testing was initiated on 6 July 2011. The waveguide distribution circuit was provided by SLAC and allows independent amplitude and phase control of adjacent pairs of

cavities. Variable Tap Offs (VTOs) were set based upon the gradient limits identified during cavity characterization. The bulk of the time spent powering the entire module was devoted to Low Level RF (LLRF) optimization and refining the Lorentz Force Detuning Compensation system. By the end of the run it was possible to control the RF amplitude and phase over 50 pulses to an RMS magnitude error of 6.0×10^{-3} % and RMS phase error of 0.005°.

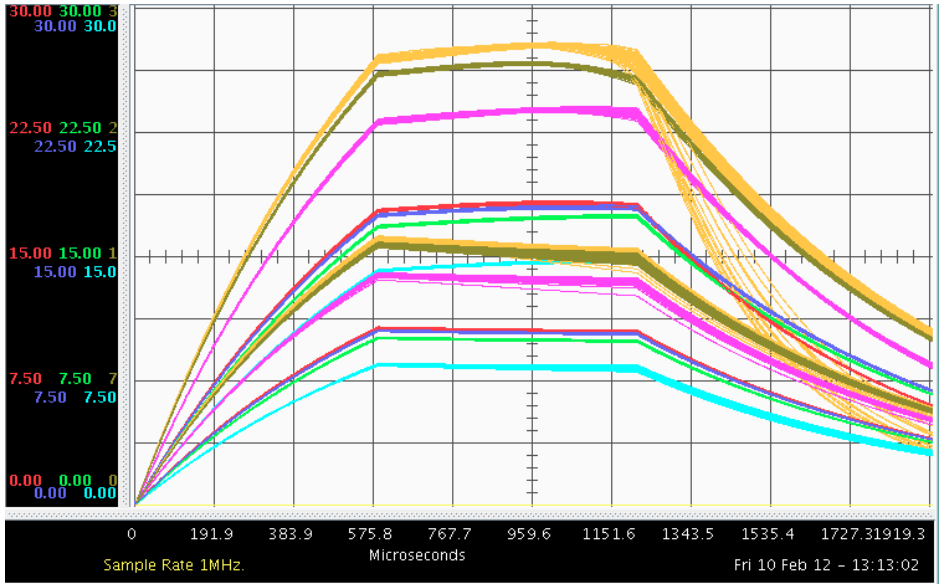

Figure 5.10: Transmitted power waveforms of all cavities pulsing at the nominal conditions just below the stable operating limit: 5 Hz, 1.3 ms pulse length (580 µs fill, 620 µs flattop) with LLRF in closed loop and LFDC disabled. One can see some quenching by the highest performing cavity and indications of Lorentz Force Detuning.

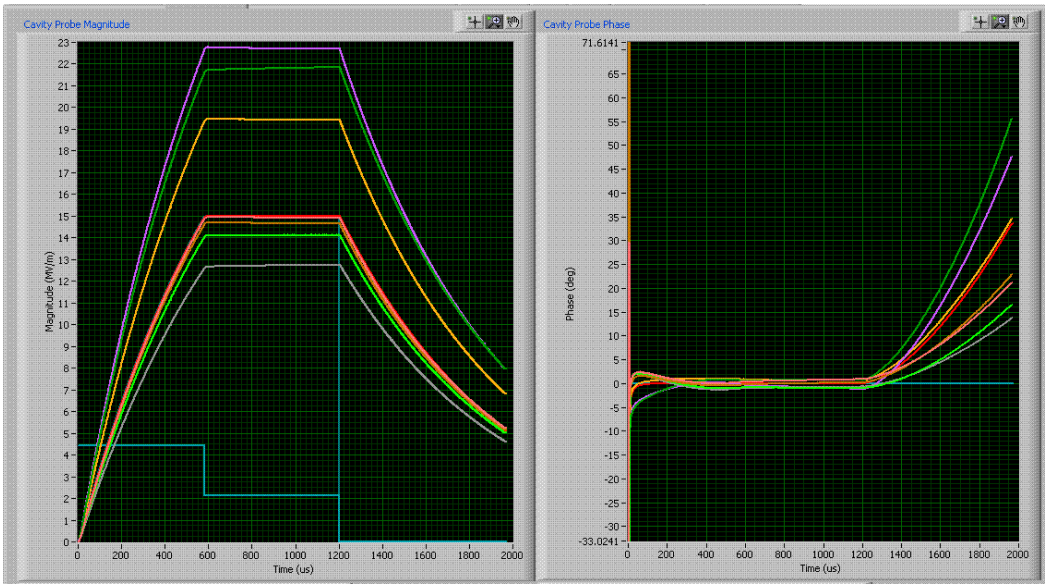

Figure 5.11: Amplitude (left) and phase (right) with both LLRF in closed loop and LFDC active for normal operation.

Much progress was made in developing a scheme to counteract the effects of Lorentz Force Detuning. An adaptive algorithm was deployed and improved which permits pulse to pulse correction. Figures 5.10, 5.11, and 5.12 show the short-term stability of the system shortly before CM1 operation ceased.

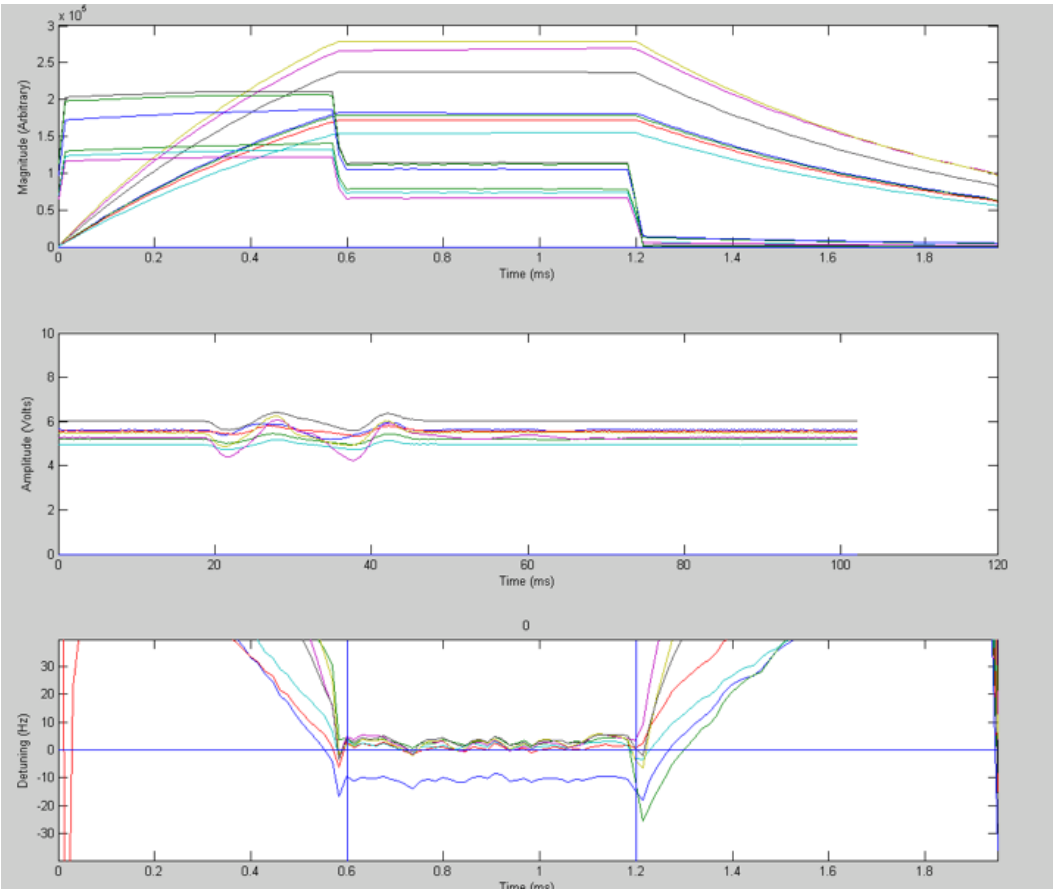

Figure 5.12: Lorentz force Detuning Compensation performance. The top plot shows the transmitted and reflected power waveforms of each of the cavities, the middle trace shows the piezo waveform applied to the individual cavities, and the bottom trace shows the detuning (or resulting lack thereof).

References

[5.1] T. Koeth, *et al.*, "Capture Cavity II at Fermilab", THP060 in Proceedings of LINAC 2006, Knoxville, TN, 2006 (http://accelconf.web.cern.ch/accelconf/l06/PAPERS/THP060.PDF)

[5.2] M. McGee, Y. Pischalnikov, "Mechanical Stability Study of Capture Cavity II at Fermilab", WEPMN103 in Proceedings of PAC07, June 2007 (http://pac07.org/proceedings/PAPERS/WEPMN103.PDF)

[5.3] T. Koeth, *et al.*, "Experience with Capture Cavity II" WEPMN094 in Proceedings of PAC07, June 2007 (http://pac07.org/proceedings/PAPERS/WEPMN094.PDF)

[5.4] T. Arkan, *et al.*, "Superconducting RF Cryomodule Production and Testing at Fermilab", TUP081 in Proceedings of Linac 2010, Tsukuba Japan, Sept. 2010 (http://accelconf.web.cern.ch/AccelConf/LINAC2010/papers/tup081.pdf)

[5.5] E. Harms, *et al.*, "RF Test Results from Cryomodule 1 at the Fermilab SRF Beam Test Facility", MOPO013 in 15th International Conf. on RF Superconductivity (SRF2011), Chicago, IL, July 2011; (http://lss.fnal.gov/archive/2011/conf/fermilab-conf-11-352-ad-td.pdf)

[5.6] A. Hocker, *et al.*, "Individual RF Test Results of the Cavities Used in the First US-built ILC-type Cryomodule", WEPPC049 in Proceedings of IPAC2012, New Orleans, LA, May 2012 (http://accelconf.web.cern.ch/AccelConf/IPAC2012/papers/WEPPC049.PDF

[5.7] E. Harms, *et al.*, "Test Results of Tesla-Style Cryomodules at Fermilab", MOPB054 in Proceedings of Linac 12, Tel Aviv Israel, Sept. 2012

6 RF systems

There are 4 separate 1.3 GHz RF systems at ASTA: a 5 MW system for the gun, two 300 KW systems for CC1 and CC2, and a 5 MW system for CM1. The 5 MW CM1 system will eventually be superseded by a 10 MW multi-beam klystron system to drive the 3-cryomodule string. Eventually there will be several 3.9 GHz RF systems at ASTA, but these are not described in this document.

6.1 High level RF

waiting for input from J. Reid…

6.2 Low level RF

The Low Level RF System for ASTA includes all controller hardware and software required to provide many accelerator functions, broken down here as subsystems: the Field Control System regulates the RF field vectors in all accelerating structures to maintain the specified beam energy and longitudinal beam emittance throughout the accelerator, the Resonance Control System regulates the superconducting cavities tuning frequency by canceling Lorentz forces generated by the RF fields and microphonics. The Master Oscillator generates frequency and phase stable multiple frequency references, the Phase Reference Lines distribute these Master Oscillator signals throughout the accelerator footprint to phase stabilized tap points.

As ASTA is a test bed for future large accelerators, the LLRF system is designed around the requirements of a large machine such as the ILC. Strong consideration is given to cost, reliability, flexibility and operability. Test results, although without beam, exceed ILC Main Linac performance requirements. Details of design considerations will be elaborated on in the following sections. See Figure 6.11 for a photograph of an installed system.

6.2.1 Field Control System

The field control system is built around a multi-stage Superheterodyne receiver, a Proportional/ Integral Controller and multi-stage up-converter. The first receiver section down-converts 1300 MHz cavity probe, forward power and reverse power signals to a 13 MHz intermediate frequency. The local oscillator signal used in this frequency mixing process is a low noise 1313 MHz signal distributed to all LLRF systems. These receivers are packaged in groups of eight channels along with one up-converter in rack mount, 1U chassis. Type N connectors on the RF inputs allow for direct input of ½" Heliax cable runs from the cryomodules. All IF receiver outputs are routed through an "8-Pack" coaxial connector and cable to the digital controller card.

ASTA supports two types of digital controllers, one a VME module (ESECON) is used in locations where a klystron drives a single cavity, the other a VXI module (MFC) [6.11] will support up to 32 cavities driven by one klystron. Both types of modules provide the functionality of first digitizing the 13 MHz IF signals, digitally down-converting this signal to a complex base-band signal, processing these real and imaginary components in a controller and then up-converting a drive signal for the klystron from the controller output. The Multi-Channel-Controller additionally generates a vector sum of all cavities from an RF group before the input of the controller and adjustable notch filters to stabilize the $7/9^{th}$ and $8/9^{th}$ π modes. All of this digital signal processing takes place in a large Field Programmable Gate Array. Placing

32 Analog to Digital Converters (ADC) along with the FPGA and Digital to Analog Converters (DAC) on a single printed circuit card is key to reducing system cost and minimizing signal group delay, allowing high proportional and integral gains. Careful choices in sampling rates and IF frequencies allow for theoretically low quantization noise and high process gain, both from signal averaging and channel averaging from the multiple cavity vector sum.

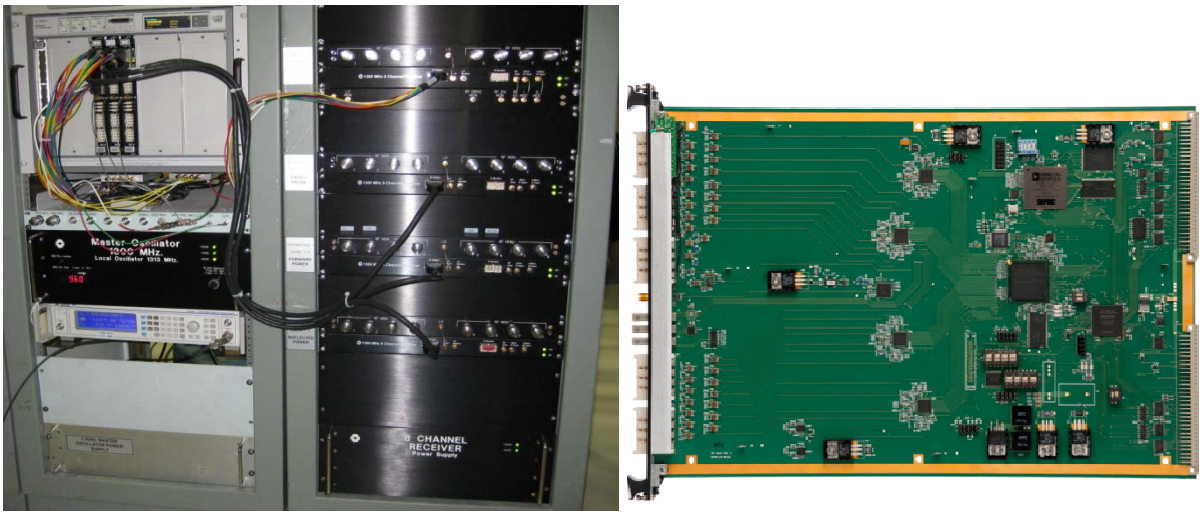

Figure 6.11: Installed LLRF System for 24 cavities per klystron and MFC Module.

6.2.2 Resonance control system

Superconducting RF cavities are designed with very high quality factors (Q) for RF efficiency. The 9-cell ASTA cavity Qs are adjustable over an order of magnitude allowing for cavity half bandwidths as narrow as 65 Hz. Dimensional changes in the cavities due to the Lorentz force, vibrations, or changes in LHe pressure can change the resonant frequency of the cavities by several bandwidths. If this detuning is not compensated, considerable additional power is required to maintain the accelerating gradient. Providing the required power overhead would significantly increase accelerator capital costs and operating costs. The Resonance Controller actively compensates for cavity detuning using a fast piezo actuator. A considerable R&D effort at ASTA has developed hardware and advanced algorithms able to limit the detuning from both repetitive disturbances such as Lorentz force detuning and from stochastic disturbances such microphonics and LHe pressure variations to the point where no significant power overhead is required [6.12].

6.2.3 Master Oscillator and Phase Reference Line

The RF systems, instrumentation, and clock systems require many low noise, frequency stable, RF signals that are harmonically related with extremely stable phase relationships. The Master Oscillator (Fig. 6.12) provides these signals. Frequency stability and low noise performance is provided by a 1.3 GHz Dielectric Resonant Oscillator phase locked to an Ultra Low Noise 10 MHz Crystal Oscillator, with only 46 femtoseconds of phase jitter. All other frequencies are generated by dividing down from the 1300 MHz reference. The Master Oscillator is enclosed in a temperature-controlled rack for added stability.

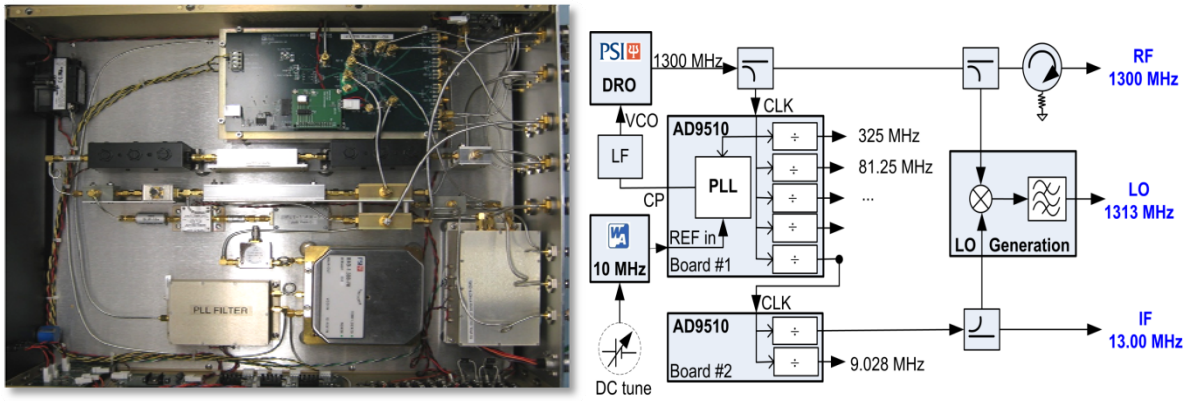

Figure 6.12: 1.3 GHz Master Oscillator

The 1.3 GHz reference signal (Fig. 6.13) is distributed down the accelerator to many subsystems. As each cavity phase is measured and controlled in relationship to this signal, the phase must be stable to better than a tenth of a degree to maintain cavity to beam phase. The ASTA reference line uses a novel phase averaging approach that is more stable and less costly than other approaches. The reference line is composed of directional couplers and 7/8" heliax cable. The reference line is shorted at one end of the line to provide reflected signals that are summed and phase averaged with the forward signals at each directional coupler. The phase drifts of the 7/8" heliax are compensated for by the phase averaging at each coupler as any change in electrical length of the coax from the shorted end of the cable will appear at the coupler as a negative phase in the forward signal and positive phase in the reflected signal. Due to imperfections of components, there are many second order effects that must be controlled. Bench performance shows better than 0.05 degree stability over a 20°C temperature range.

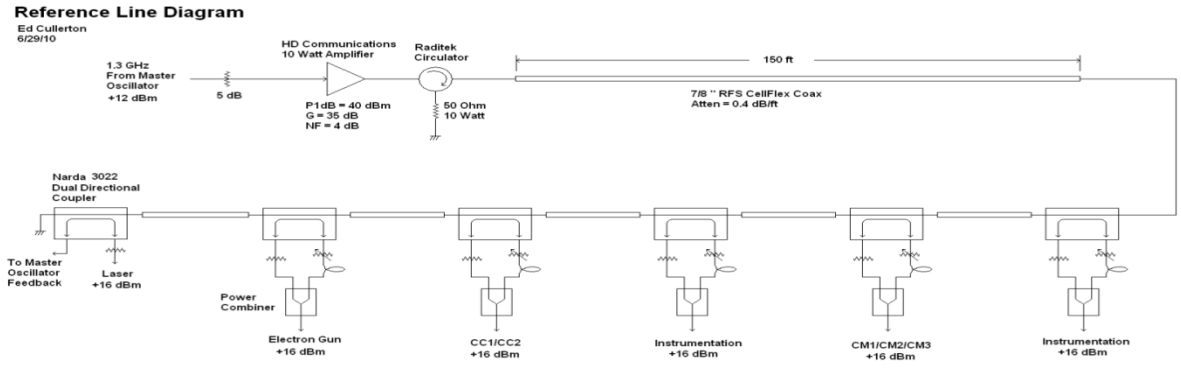

Figure 6.13 Phase Reference Line

References

[6.11] P. Varghese *et al.*, "A Vector Control And Data Acquisition System For The Multicavity LLRF System For Cryomodule 1 At Fermilab", MOP084 in LINAC2010 Tsukuba, Japan, Sept. 2010 (http://accelconf.web.cern.ch/accelconf/LINAC2010/papers/mop084.pdf)

[6.12] W. Schappert, Y. Pischalnikov, "Adaptive Compensation for Lorentz Force Detuning IN Superconducting RF Cavities", FRIOA01 in Proceedings of SRF2011, Chicago, IL, July 2011; (http://lss.fnal.gov/archive/test-tm/2000/fermilab-tm-2476-td.pdf)

7 Instrumentation

7.1 Beam position monitors

waiting for input from N. Eddy …

7.2 Wall current monitors

waiting for input from N. Eddy …

7.3 Beam profile monitors

The beam transverse intensity distributions will be measured by profile monitors located in 6-port vacuum crosses. These devices, including internal vacuum hardware, optical transport, and mechanical actuators were fabricated by Radiabeam Technologies. Drawings of these monitors are shown in Figures 7.21 – 7.23.

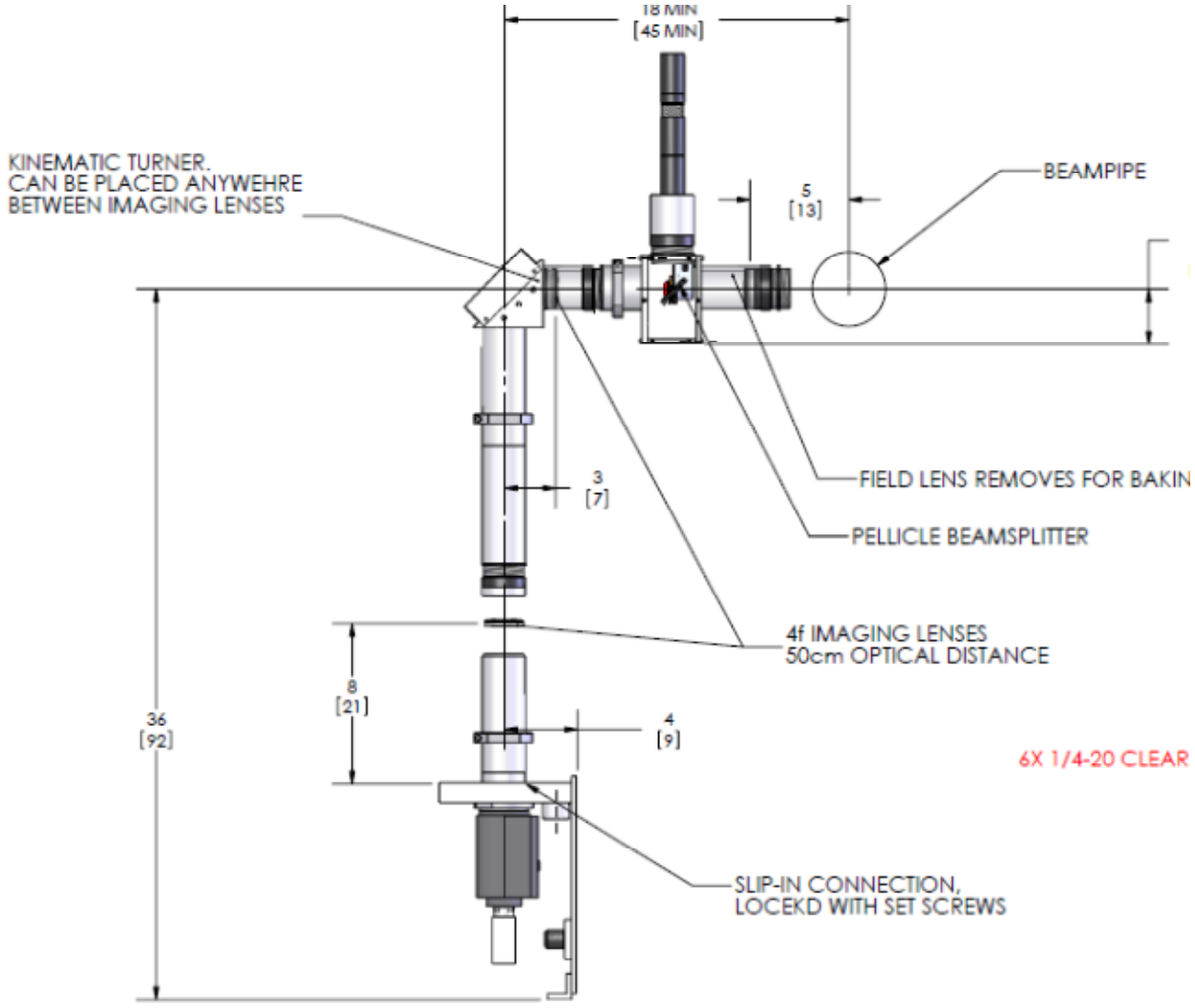

Figure 7.21: Optical channel of Radiabeam profile monitor.

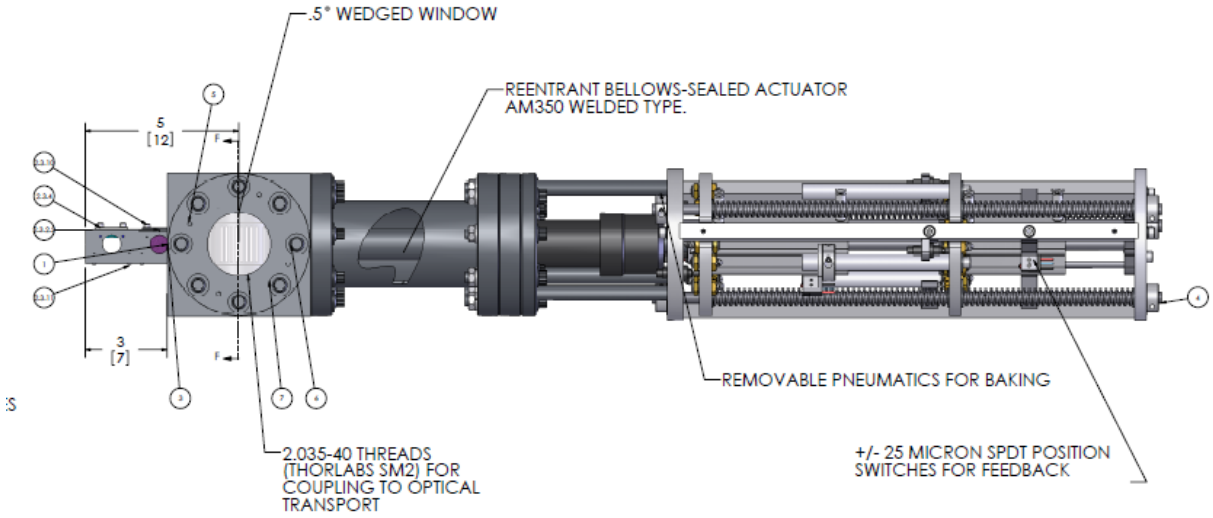

Figure 7.22: Actuator assembly of Radiabeam profile monitor.

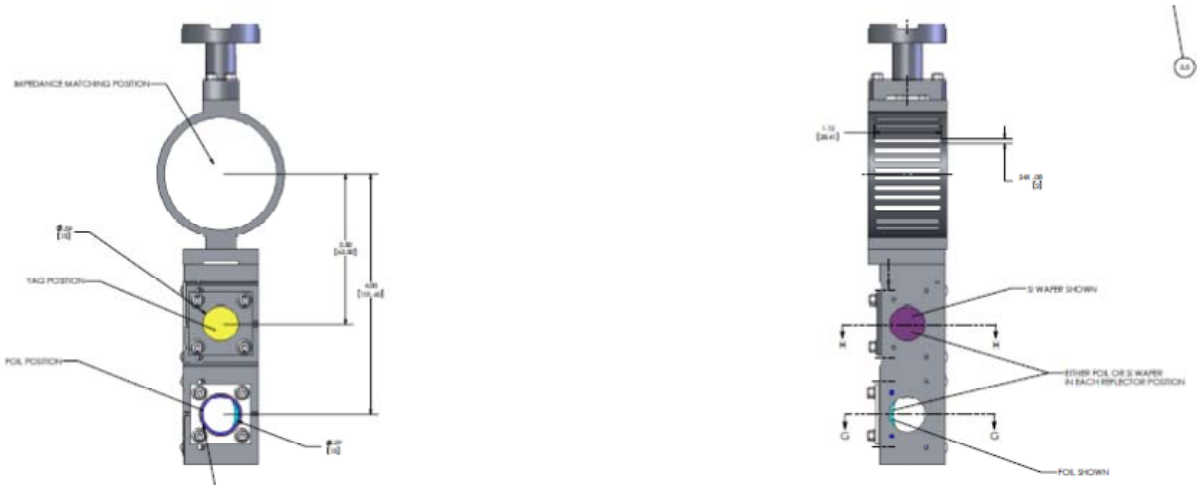

Figure 7.23: Internal components of Radiabeam profile monitor. Calibration target is not shown.

A prototype was tested at the Fermilab A0 photoinjector [7.21] [7.22] and the project-specified 1σ resolution of <20 μm was obtained. Each monitor contains a Ce-doped 100 μm thick crystalline yttrium aluminum garnet (YAG) screen or a 100 μm thick crystalline lutetium-yttrium oxyorthosilicate (LYSO) screen to produce scintillation light, a 1 μm thick Al screen for optical transition radiation (OTR) production, and a target screen for calibration. These screens are at right angles to the beam and are followed by a 45° mirror to deflect optical light into an optical transport. This arrangement avoids the loss of resolution due to depth-of-field when only a single image-producing screen is placed at 45° to the beam direction. This initial configuration that involves two OTR sources from the thin foil (in focus) and 45 degree mirror (out of focus) is being evaluated. Processing of these images with a 2-Gaussian fit with input for the defocused image is the present plan. A second method of shifting the field lens to focus at either the scintillator screen plane or the single mirror plane has been tested successfully. The remote

control of this lens position would then allow switching the optical focus between the scintillator screen position and the single OTR source position.

A 4-position actuator (two 2-position actuators piggy-backed) controls which of the 3 objects (scintillation screen, OTR screen, target) are inserted in the beamline. The fourth position is the "out" position in which an RF beam shield is inserted to minimize beam impedance from the vacuum ports. The combination of these radiation converter screens and two filter wheels with selectable neutral density filters, band pass filters, and polarizers provides a very flexible imaging system. The system addresses imaging single micropulse charges from 20-3200 pC, micropulse numbers from 1-100, the factor of 100 difference in the OTR and scintillator yields per unit charge, the mitigation of the microbunching instability effects on OTR should it exist after bunch compression, the saturation of the scintillator mechanism for charge areal densities greater than 10 $fC/\mu m^2$, the use of linearly polarized OTR components for more reliable image sizes, and the reduction of bremsstrahlung source strength from the screens and mirrors. The cameras used to record the image are 5-megapixel CCD cameras purchased from Allied Vision Technologies (Prosilica GC2450 model), and the readout protocol is GigE. Image processing software will provide basic beam size and position parameters on-line to the operators and experimenters. There will be 9 of these profile monitors in the primary injector beamline, and 9 additional profile monitors in the high energy beamlines.

Using 15 MeV A0PI beam, The YAG:Ce example in Fig 7.24a shows the image for 5 bunches at 500 pC per bunch with an ND1 filter to attenuate the light. The measured projected profile sigma width is 160 μm in the region of interest (ROI). The profile was fit well with a single-Gaussian peak. By using a flat beam transform and irising the drive laser we were able to make a 46 x 295 μm beam image involving only 15 pC of charge in one bunch as shown at the right in Fig. 7.24b. This demonstrates our low-charge imaging capability.

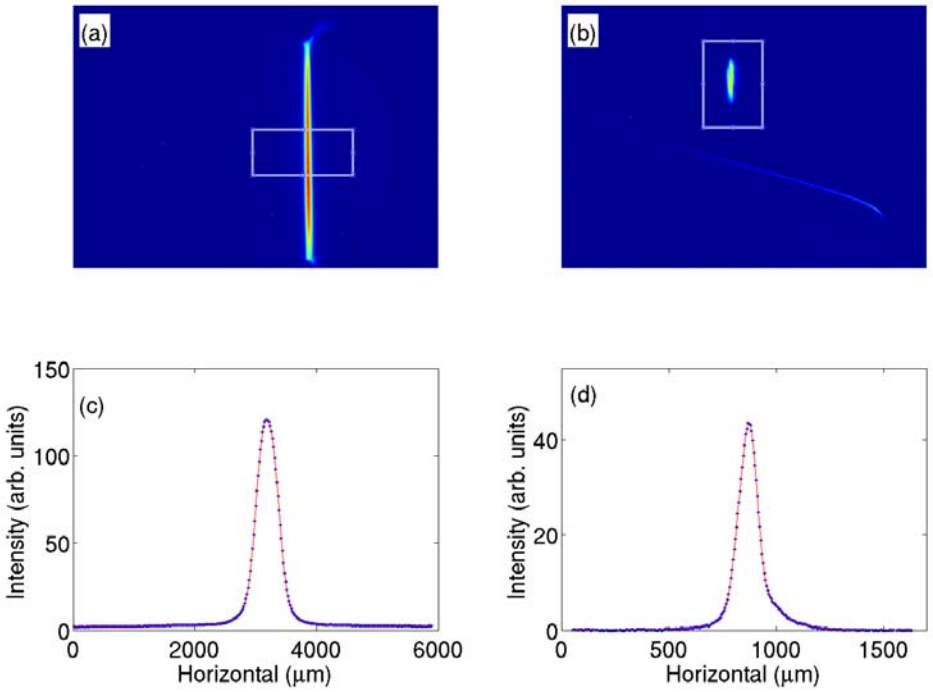

Figure 7.24: Composite display of a) the vertical band image from the YAG:Ce crystal and c) projected x profile (blue) and its Gaussian profile fit (red curve) and b) the image of the 46 μm x 295 μm beam spot with only 15 pC and d) the corresponding projected profile and Gaussian fit.

There will be 2 additional profile monitors in the injection beamline which will be used for emittance measurements using the "slits" technique. These devices are modified from an A0PI design, and the screens and slits are mounted on rotatable stepping motors to ensure that the slits array is at right angles to the beam.

There will be 1 additional profile monitor on the "9-way" cross to measure the profile of the ~5 MeV beam just downstream of the electron gun. This profile monitor contains only a YAG screen and calibration target.

References

[7.21] A. Lumpkin, *et al.*, "Initial Beam-profiling Tests with the NML Prototype Station at the Fermilab A0 Photoinjector", MOP219 in NA-PAC11, New York, NY, Dec. 2011 (http://accelconf.web.cern.ch/AccelConf/PAC2011/papers/mop219.pdf)

[7.22] A. Johnson, *et al.*, "ASTA/NML Transverse Profile Station: Testing and Installation", Beams-Doc-4020, Dec. 2011 (https://beamdocs.fnal.gov/AD/DocDB/0040/004020/001/TPM_rev2.pdf

8 Lattice calculations and simulations

Extensive lattice calculations and beam simulations have been performed to validate the ASTA beamline design under a wide range of beam parameters and configurations [8.1] [8.2]. Both ASTRA [8.3] and Impact-T [8.4] are used to simulate beam to the downstream end of the 2nd acceleration cavity (8.2 m from the photocathode); Elegant [8.5] is used to calculate single particle (low intensity) beam dynamics from 8.2 m to the high energy dump; Impact-Z [8.6] is used to simulate multiparticle (high intensity) beam dynamics from 8.2 m to the high energy beam dump and includes the effects of space charge and coherent synchrotron radiation. CSRtrack [8.7] is used to simulate beam through the magnetic chicanes. Figure 8.1 shows where in the beamlines the different tracking codes are used.

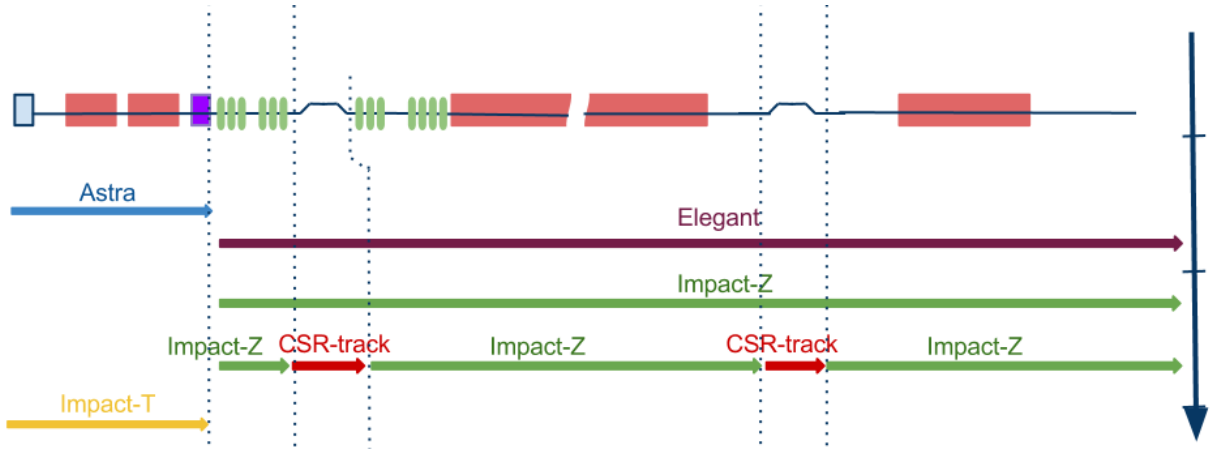

Figure 8.1: Location in beamlines where different particle tracking algorithms are used. Impact-T allows for cylindrically asymmetric beams at the photocathode, as is necessary for flat-beam transformations.

As examples, Figure 8.2 shows results from typical lattice and beam size calculations from Elegant and Impact-Z. Figure 8.3 shows the longitudinal phase space beam distributions before and after bunch compression in the injector chicane for single particle dynamics (no collective effects). Figure 8.4 shows a comparison between Impact-Z and CSRtrack in simulating longitudinal phase space through the low energy bunch compressor. The plots on the left side are generated by Impact-Z and the plots on the right side are generated by CSRtrack.

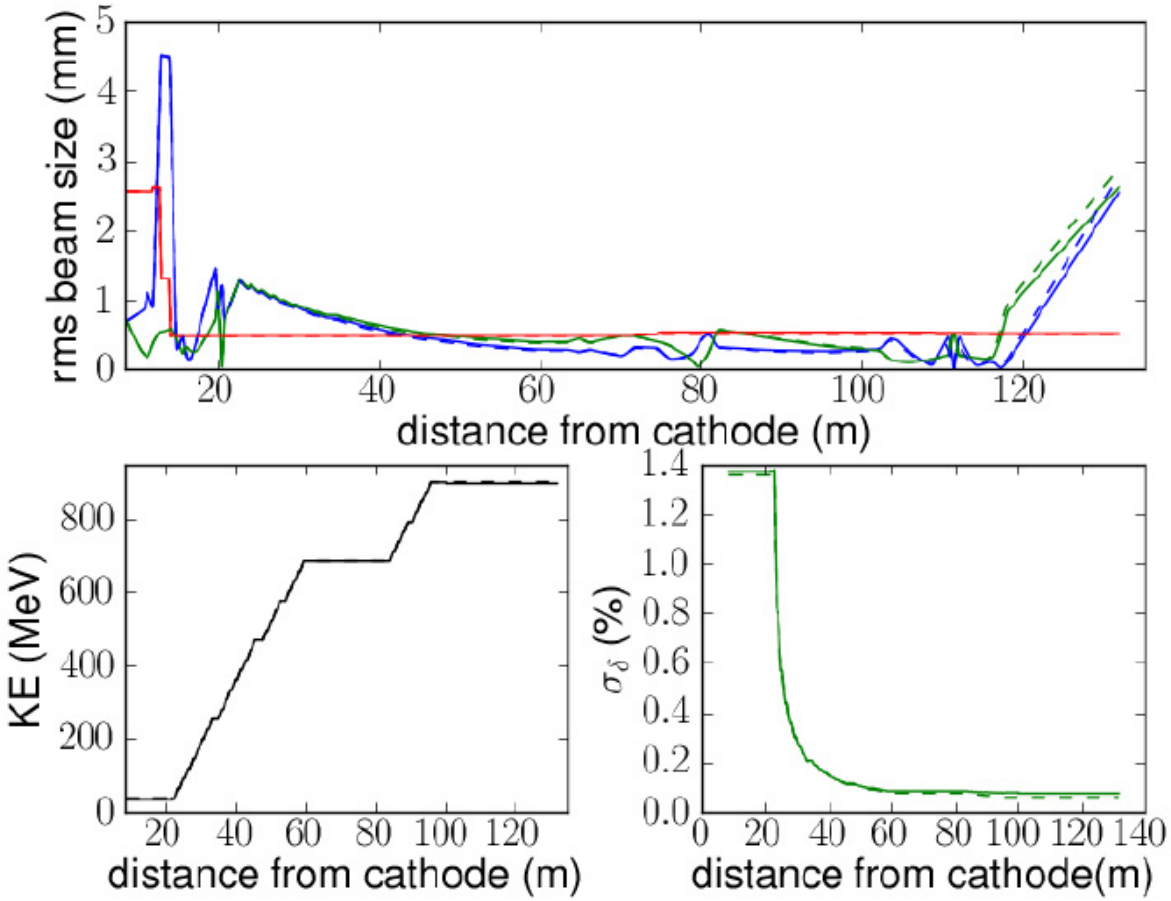

Figure 8.2: Top plot shows beam size from 8.2 m to the high energy dump in the 3-cryomodule configuration followed by a 2nd high energy bunch compressor and 4th cryomodule. Green is vertical, blue is horizontal, and red is longitudinal. Bottom plots show beam energy and energy spread.

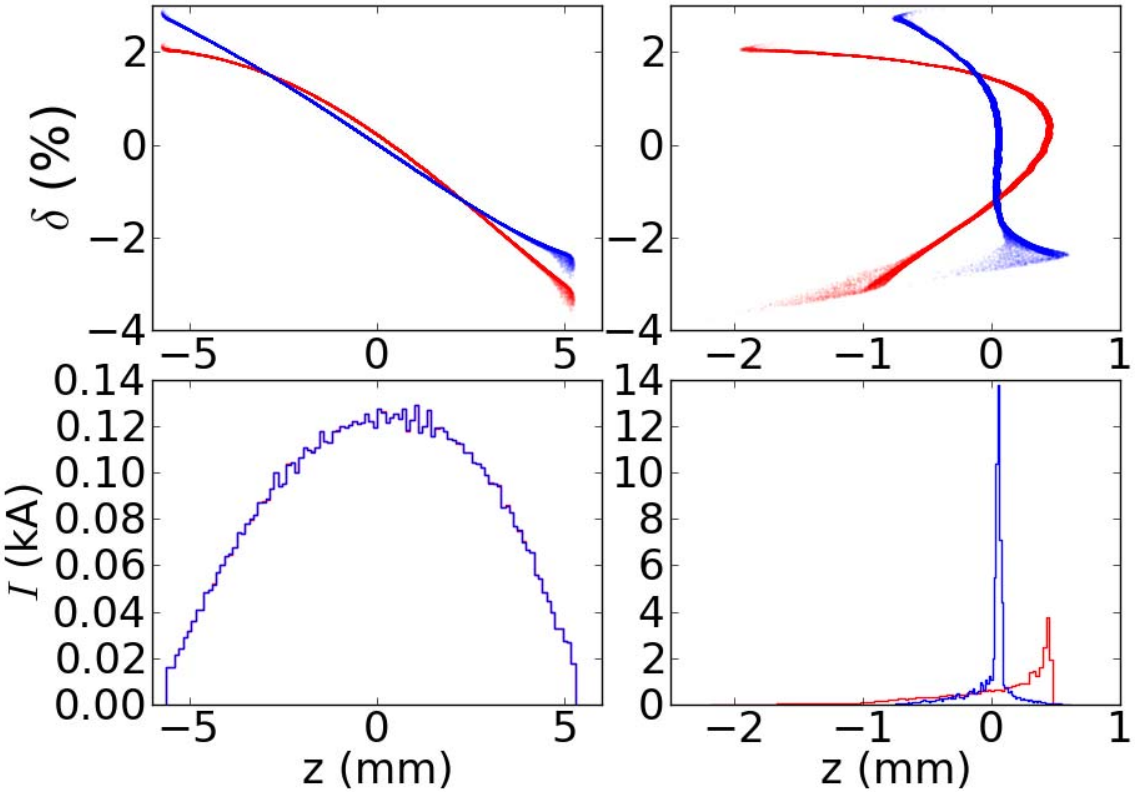

Figure 8.3: Top plots show longitudinal phase before and after bunch compression. Bottom plots show projection on the z-axis. Blue plots are with bunch linearization with a 3.9 GHz cavity included; red plots without. Bunch charge is 3.2 nC. Collective effects are not included in these plots.

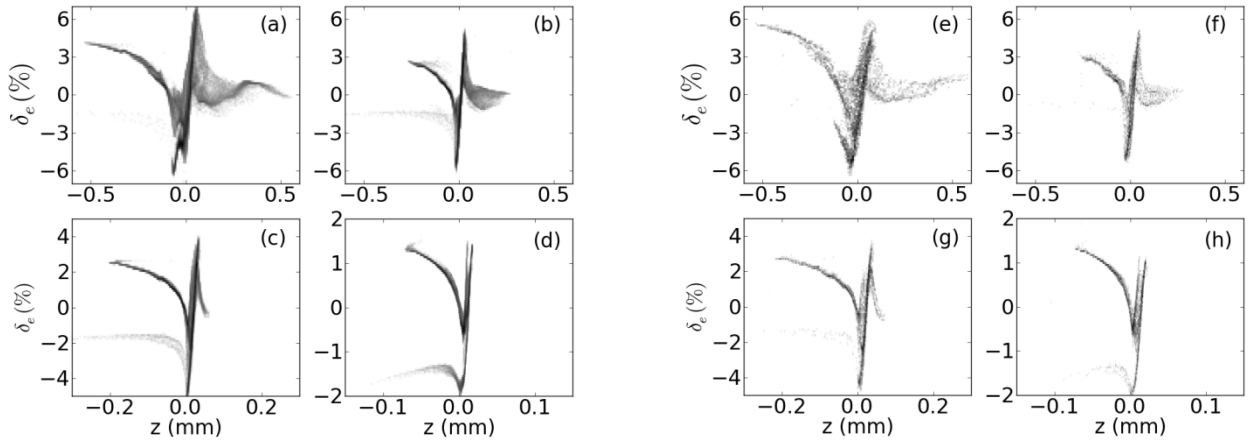

Figure 8.4: Comparison of Impact-Z and CSRtrack for low energy bunch compression. The 4 plots on the left are generated by Impact-Z for 3.2 nC, 1 nC, 250 pC, and 20 pC. The 4 plots on the right are generated by CSRtrack for 3.2 nC, 1 nC, 250 pC, and 20 pC.

References

[8.1] C. Prokop, *et al.*, "Start-to-end Beam Dynamics Simulations for the SRF Accelerator Test Facility at Fermilab", WEP036 in NA-PAC11, New York, NY, March 2011 (http://accelconf.web.cern.ch/AccelConf/PAC2011/papers/wep036.pdf)

[8.2] C. Prokop, *et al.*, "High energy Lattice for First-beam Operation of the SRF Test Accelerator at NML", Fermilab-TM-2516-APC, March 2012 (http://lss.fnal.gov/archive/test-tm/2000/fermilab-tm-2516-apc.shtml)

[8.3] K. Floettman, "ASTRA – A Space Charge Tracking Algorithm" (http://www.desy.de/~mpyflo/)

[8.4] J. Qiang, "Impact-T: A 3D Parallel Particle Tracking Code in Time Domain" (http://amac.lbl.gov/~jiqiang/IMPACT-T/

[8.5] "Elegant – Electron Generation and Tracking" (http://www.aps.anl.gov/Accelerator_Systems_Division/Accelerator_Operations_Physics/manuals/elegant_latest/elegant.html)

[8.6] "Impact-Z – Integrated Map and Particle Accelerator Tracking Code",(http://amac.lbl.gov/~jiqiang/IMPACT)

[8.7] "CSRtrack Version 1.1 User's Manual" (http://www.desy.de/fel-beam/csrtrack/files/CSRtrack_User_Guide_1.100_01.pdf

9 Machine protection system

9.1 Overview

The beam at ASTA will need systems to protect critical components from beam induced damage such as beam pipe collision and excessive beam losses. With three cryomodules installed the facility will be capable of generating electron beam energies of 810 MeV and an average beam power that approaches 40 KW. Operation at full intensity can deposit enough energy in the beampipe to melt it, therefore a robust Machine Protection System (MPS) is required to mitigate effects due to such large damage potentials. The MPS must identify hazardous conditions and then take the appropriate action before damage is caused. Since the loss of a single bunch train can result in significant damage, the MPS must also be able to interrupt the beam within a macro-pulse and keep the number of bunches below the damage potential once the protection system reacts. With the a bunch frequency of 3 MHz this necessitates a reaction time in the range of 1-2 μs with cable delay included for the 134 metre long machine. The MPS will use the status of critical sub-systems and losses measured by a fast Beam Loss Monitor (BLM) system, using scintillators and photomultiplier tubes (PMT) to identify potential faults. Once a fault is observed, the MPS can then stop or reduce beam intensity by removing the permit from different beam actuators.

From a machine protection point of view, the dump locations describe the final destination of the beam that traverses a path along the beam-line. These paths are termed operation modes and are validated by the MPS before the beam permit is released. The MPS validates these paths by monitoring all critical devices and diagnostics along the path and ensuring that they are all in good status and ready to receive beam at the requested intensity. The machine will also be capable of operating over a wide range of beam parameters as long as the total beam power remains below the limit of the beam dump capability and satisfies radiation shielding requirements. For machine protection purposes several beam modes have been defined -- the beam mode sets limits on the number of bunches and therefore the intensity. Initially the following two modes will be active in the system:

- Low intensity mode – which allows the minimal beam intensity needed for OTR/YAG and BPM diagnostics. This is below the threshold potential for beam induced damage. In this mode there is no fast reaction to beam loss within a bunch train.
- High intensity mode – which does not impose a limit on the number of bunches, but enables fast intra-train protection by the MPS.

The simplified block diagram of the MPS is shown in Figure 9.1. The system is divided into three functional layers which have connections to several external devices and sub-systems. The top layer (shown on left) comprises signal providers such as fast beam loss monitors, RF signals, quench protection, toroid transmission, vacuum, magnet power supplies and more. All devices in this category send status information to the MPS logic layer (permit system). Only simple digital signals (e.g. on-off, OK-not OK) are transmitted. All devices or subsystems that are determined to be pertinent to protecting the machine or necessary for machine configuration are included here. The state of the machine is determined from this comprehensive overview of the inputs and allowable operation modes are determined based on this information by the middle logic layer.

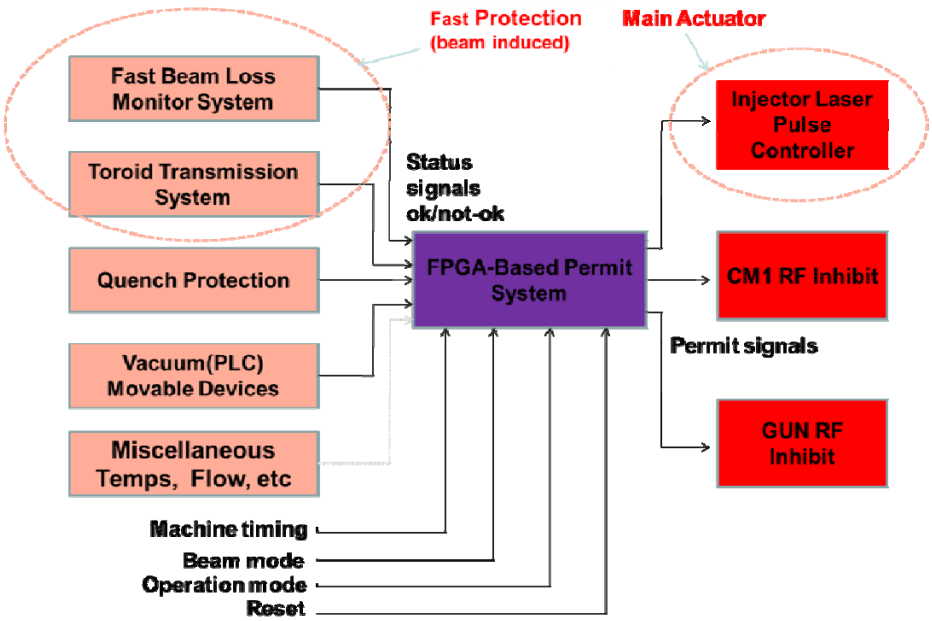

Figure 9.1: MPS block diagram

The main goals for the MPS system as a whole are:

- Provide precise protection of all critical components by first determining the fault severity (high, intermediate, etc.) and then taking the appropriate action to avoid damage.
- Allow for high availability by ensuring that the maximum requested beam intensity is allowed for the detected fault severity.
- Monitor MPS components and perform periodic self-checks in order to ensure robustness and a high level of reliability.
- Provide well-integrated, user-friendly tools for fault visualization, control, and post-mortem analysis.

The permit system part of the MPS is capable of handling events on all time scales relevant to the machine. This layer is FPGA based and is thus fully programmable and handles complex logic tasks. The logic here will be designed to ensure safe operating conditions by monitoring the status of critical devices and by imposing limits on the beam power. It prohibits beam production by disabling the gun RF and the injector laser unless the requirements for the specific predefined modes are fulfilled when that mode is requested. The final layer of the system consists of the main beam actuators. This comprises all of the points where the MPS logic may act on the operation of the machine and prevent beam from being produced or transported -- the main actuator being the injector laser. When any of the non- masked inputs signal an alarm status the MPS permit system (logic layer) can do one of several things based on the severity of the fault: i.e. switch off the injector laser to suppress the production of new bunches, reduce the intensity by dialing back the number of bunches, or inhibit the RF power from the gun or first cryomodule (CM1) as a precaution against transport of dark current from the RF gun.

The MPS requires server support for the various hardware systems to view, configure and diagnose the system. There are currently several servers under development for the beam loss monitor system and the laser pulse controller. These servers are implemented using the PowerPC

5500 series boards running VxWorks 6.4 and implementing the ACNET protocol. Some of the main requirements for these servers include:

- Time-stamping at a sub-microsecond resolution in order to allow for data correlation.
- Circular buffers that are logged using ACNET data loggers and thus provide a repository used for post-mortem analysis.

9.2 Laser pulse controller

The main actuator for the MPS is the injector laser pulse control system shown in Figure 9.2. This is the device that controls the number and the spacing of bunches in a macro-pulse by picking single laser pulses out of a 81.25 MHz train using a Pockels cell. It is a VME based board with a fully programmable FPGA. It has inputs for the requested beam modes defined by the logic layer of the MPS, the MPS permit signal, the 3 MHz machine timing, and a macro-pulse trigger. It has control outputs for the Pockels cell driver, a mechanical shutter, and a first bunch timing signal. From the protection system point of view the pulse controller is used to:

- Block the Pockels cell pulse kickers as long as **any** MPS input is in an alarm state.
- Enforce the limit on the number of bunches as given by the currently selected beam mode.
- Close the laser shutter on request of the MPS. This may happen when there is no valid operation mode or when some combination of loss monitors exceed thresholds which trigger a dump condition.

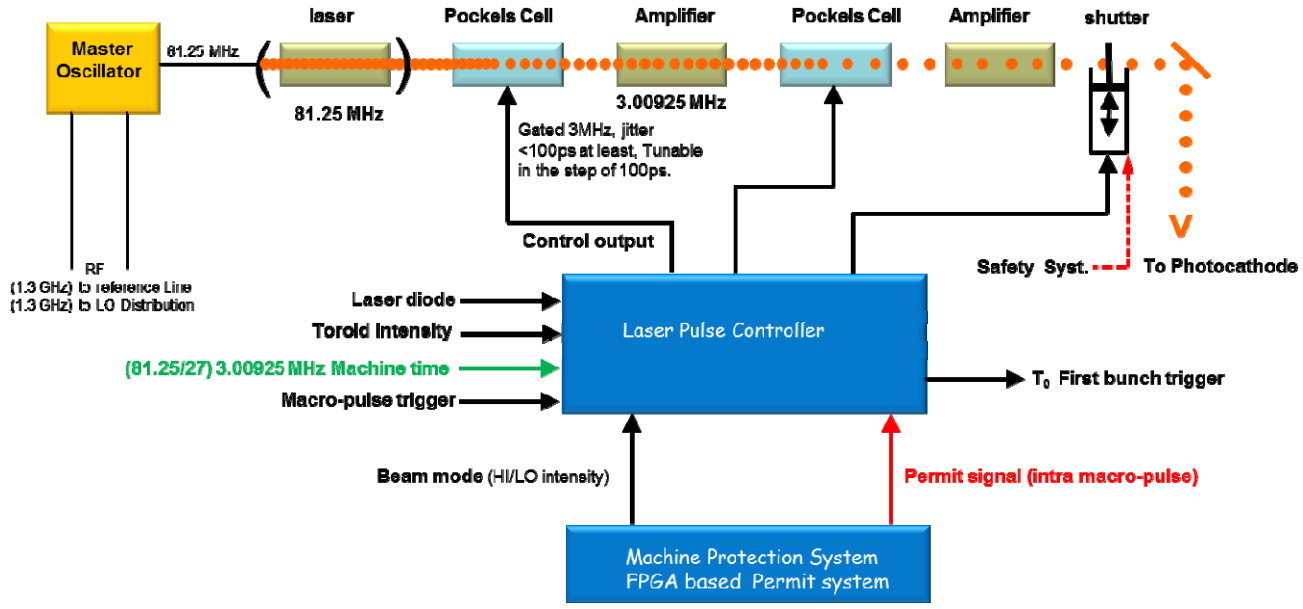

Figure 9.9: Laser pulse controller system

9.3 Fast beam loss monitors

ASTA will use about 40 BLMs for diagnostics and machine protection. The monitors are made of plastic scintillator instrumented with PMTs. The BLMs will serve the dual purpose as an accelerator diagnostic for tuning and as the primary detector for the fast machine protection

system. The monitors will deliver a measurement of beam and dark current losses to the control system as well as generate a fast alarm signal when the beam losses exceed user-defined thresholds. The time resolution of the loss measurement provides the ability to distinguish single bunches within each macro pulse. This requires a sampling frequency of at least 3 MHz (the bunching frequency of the machine) with a repetition rate of 5 Hz. The main requirements for the BLM system are:

- Provide both machine protection and diagnostic functions.
- Instantaneous read-back of beam loss.
- Digital output for integrating and logarithmic signal (16 bit)
- Built in self-test and on-board signal injection for testing of monitors between pulses.
- FPGA controlled.
- Local data buffer.
- VME interface to ACNET control system.
- Continuous and pulsed monitoring.
- Wide dynamic range.

9.3.1 Loss Monitor Design and Specifications

The loss monitors are made from a Y-shaped plastic scintillator (EJ-208). The PMT type was selected for high linearity and excellent gain stability (typically less than 5% drift in the first 24 hours after power on). The unit includes a low-power embedded high voltage divider with a typical HV supply current of 15 µA at 1000 volts. The embedded high-voltage divider employs a transistorized voltage divider for best linearity at the lowest power consumption. It supports high anode currents (I > 100 µA). A fast green LED is embedded within the plastic for testing and calibration. All units are housed in a steel magnetic shield made of 0.5 mm thick µ-metal. See Figure 9.3.

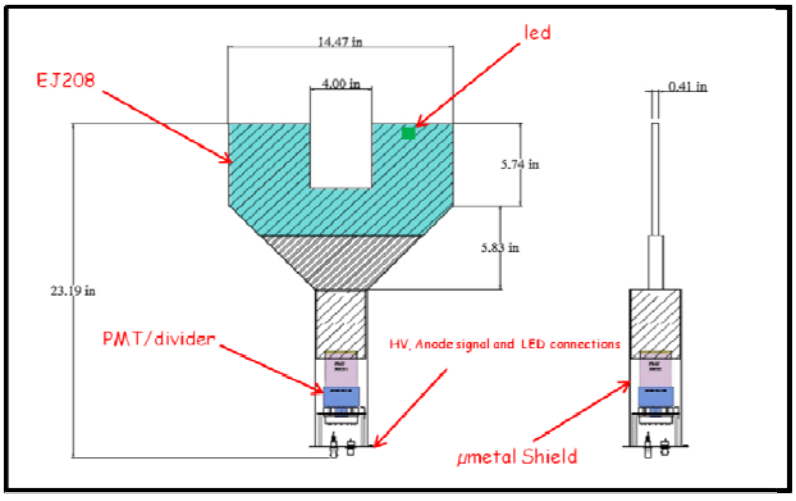

Figure 9.10: Beam loss monitor

The embedded LED in the plastic provides an operability check of each monitor. An LED driver initiates a test pulse shortly before or after each RF pulse at the machine repetition rate of 5 Hz, and the amplitude of the test pulse is adjustable. To ensure that the PMTs are connected and functioning properly, the high voltage of each PMT or its current consumption is monitored. All loss monitors are individually powered. Table 9.1 lists monitor characteristics.

Table 9.1: BLM parameters.

Parameter	Symbol	Min	Typ.	Max	Comment
Performance					
Energy resolution at 478 KeV			70%		Cs-137 Compton corner
PMT gain			213 k		HV = 1000 V
PMT gain exponent			5.68		HV = 750 to 1200 V
Scintillator brightness			76 p.e/MeV		
Detector sensitivity	$\mathbf{S_p}$		7.0 pC/MeV		HV = 1200 V
			43.7 C/J		HV = 1200 V
Dose rate sensitivity	$\mathbf{S_d}$		46μA/(R/hr)		HV = 1200 V
Max dose rate (I = 50μA)		D_{max}	1.09 R/hr		HV = 1200 V
Detector sensitivity	$\mathbf{S_p}$		0.30 pC/MeV		HV = 700 V
			1.88 C/J		HV = 700 V
Dose rate sensitivity	S_p		1.98μA/(R/hr)		HV = 700 V
Max dose rate (I = 50μA)		$\mathbf{D_{max}}$	25 R/hr		HV = 700 V
LED					
Type			IF-E93, green, fast LED		
Forward voltage			3.5 V		IF = 5 mA
Ballast resistor		RB	1.0 kΩ		
HV- subsystem					
HV range		HV	700 V	1400 V	Negative HV
HV supply current		I_{HV}	15μA	18μA	HV = 1000 V
Anode resistor to GND		R_A	100 kΩ		
Environmental					
Operating temperature		5° C		60° C	

9.3.2 Theory of operation

The PMT is powered using negative high voltage, and the anode is DC-coupled to its BNC connector. The last dynode is sent to its BNC connector via a 100 Ω resistor and a 1 nF capacitor. The DC anode current of the PMT can be related to the dose rate deposited in the plastic scintillator as follows:

$I = S_P * m * \dot{D}$,

where S_p is the energy calibration, expressed in pC/MeV for convenience when measuring energy spectra, or C/J for dosimetry. (1 pC/MeV = 6.24 C/J) The mass of the plastic scintillator $m \approx 0.380\ kg$, and $\dot{D}$ is the dose rate caused by the radiation field. (1 Rad/hr = 2.78E-6 J/kg- s) The anode will support currents up 50 µA DC with minimal gain shift, < 2%. Hence the maximum dose rate or full scale range can be computed as

$$\dot{D} = I_{max}/(S_P * m)$$

And the dose range can be adjusted via the PMT gain and high voltage setting.

9.3.3 Beam Loss Monitor Test Results

The beam loss monitor prototype was tested with electron beam at the A0 Photoinjector. Figure 9.4 shows the BLM signal with 40 bunches with about 250 pC per bunch. The broadening in the signal was due to the inconveniently long (310 ft) RG58 cable used during the test. It is expected that the widths will be ~ 10-20 ns with the appropriate length of cable. The PMT voltage used during the measurement was ~ 700 volts. The dark current background in this case was very small but some measure of dark current is anticipated and will be considered in the system design. Figure 9.5 shows a case where a measurable amount of dark current was produced at the gun along with 10 bunches.

Figure 9.11: Signal from 40 bunches, 250 pC/bunch.

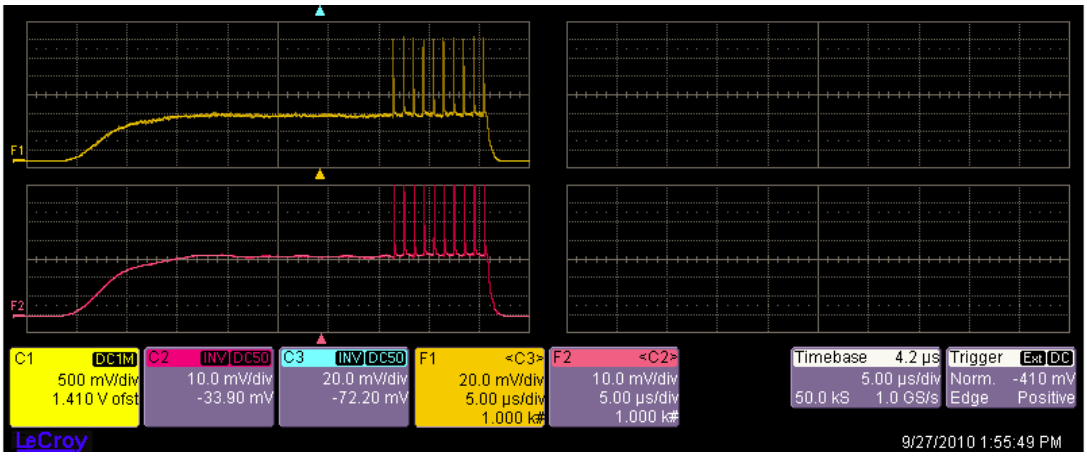

Figure 9.12: 10 bunches riding on dark current background

9.3.4 Beam Loss Monitor Signal Processing

The BLM signals will be continuously digitized with the full bunch frequency of the machine (3 MHz). Immediately after each sample "S" is available from the ADC, it is to be compared to a "single bunch" and a "multi-bunch" threshold T_s and T_m . An alarm will be signaled directly if $S > T_s$ or if $S > T_m$, a counter C incremented, and an alarm raised if C exceeds a configurable threshold T_c . The counter C will reset to zero between the macro-pulses. In a time window of ~1-2 ms surrounding the full RF pulse, the ADC samples will be stored in a buffer and made available to the control system on a pulse by pulse basis at 5 Hz. Within this time window, an integrated signal "I" is continuously calculated and compared to a threshold T_i ; exceeding the threshold raises an alarm. Figure 9.6 is a block diagram concept of the entire loss monitor system.

Due to the time delay of data processing of an alarm signal from an FPGA a fast analog comparator circuit is needed to provide a fast reaction time to high losses. The alarm signals from the comparator and the FPGA will be OR-ed and the result sent to the MPS. The reaction time to losses is mainly determined by the propagation time of the signal in the cable. The overall length of the ASTA is 133.5 meters so based on expected FPGA processing times (~1 ns) and cable delays of ~0.4 µs it is reasonable to expect a response time of 1-2 µs from the protection system overall.

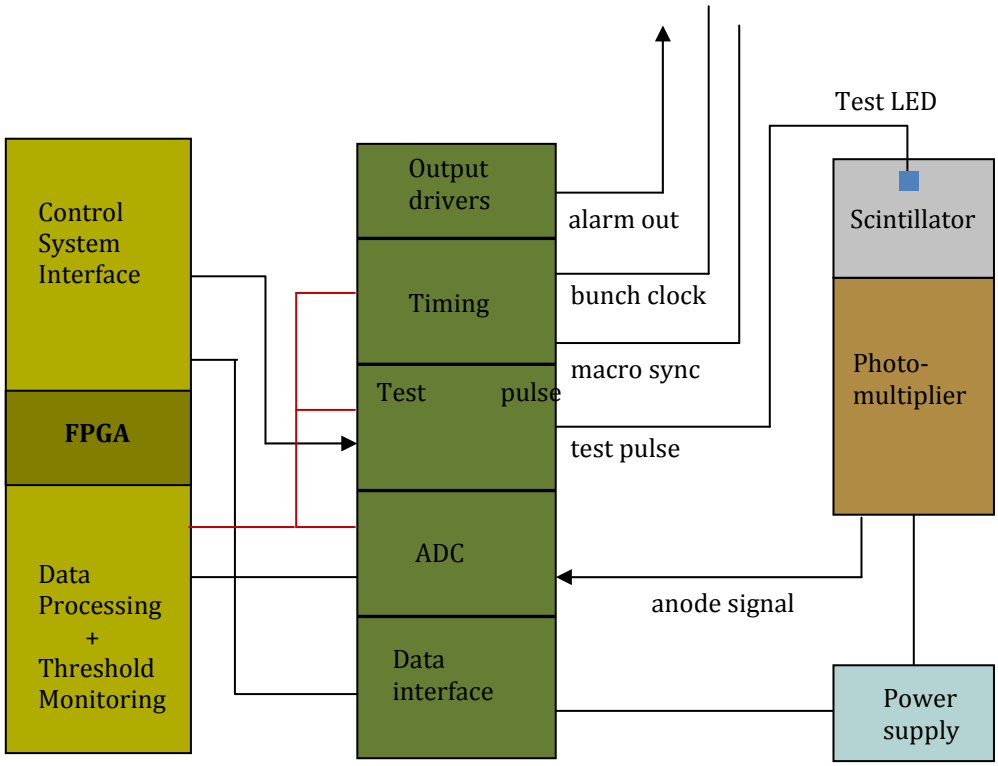

Figure 9.13: BLM system diagram

9.4 Cryogenic loss monitors

Although loss monitors are typically one of the main diagnostics for protecting the accelerator from beam induced damage, most accelerator facilities do not cover the cold sections of the machine with loss monitors. To address this issue a Cryogenic Loss Monitor (CLM) ionization chamber capable of operation in the cold sections of a cryomodule has been developed and will be installed and tested [9.1]. The monitor electronics have been optimized to be sensitive to DC losses and the signals from these devices will be used to study and quantify dark current losses in particular, as shown in Figure 9.7. In order to increase the resolution bandwidth and the response time of the devices a new scheme which uses an FPGA based Time-to-Digital converter (TDC) method is implemented [9.2] instead of a standard pulse counting method. This potentially renders these monitors as useful devices for both dark current monitoring and machine protection. The monitors under consideration are custom built detectors. They are an all-metal design which makes them intrinsically radiation hard and suitable for operation at 5°K to 350°K.

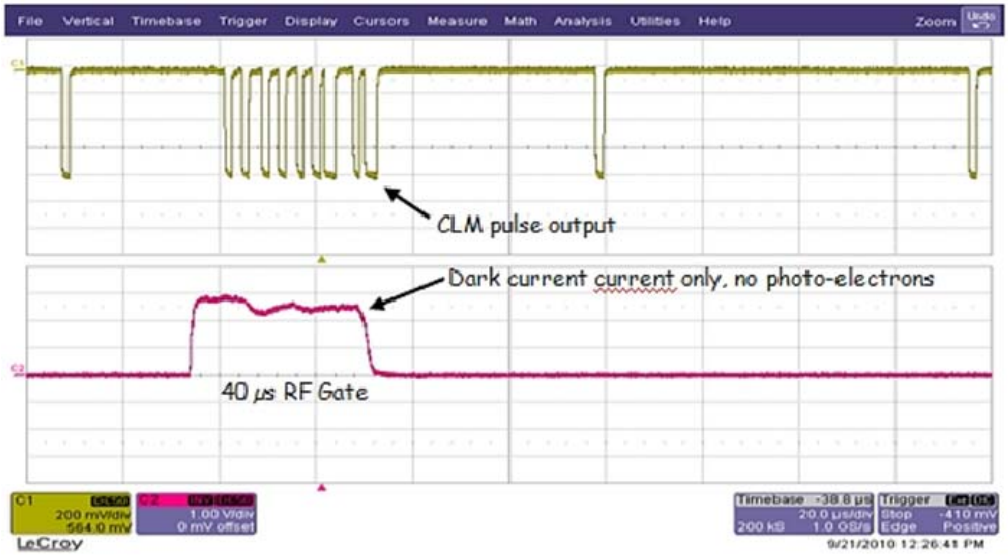

Figure 9.14: Reaction of CLM to dark current losses in a test beam.

References

[9.1] A. Warner, J. Wu, "Cryogenic Loss Monitors with FPGA TDC Signal Processing", in TIPP2011, Chicago, IL, June 2011; (http://lss.fnal.gov/archive/2011/pub/fermilab-pub-11-467-ad.pdf)

[9.2] A. Warner, J. Wu, "A Novel Digitization Scheme with FPGA-based TDC for Beam Loss Monitors Operating at Cryogenic Temperatures", in 2011 IEEE Nuclear Science Symposium and Medical Imaging Conference, Valencia, Spain, Oct. 2011; (http://lss.fnal.gov/archive/2011/conf/fermilab-conf-11-587-e.pdf)

10 Controls

10.1 Timing

ASTA makes full use of all features of the Fermilab Accelerator Controls system (ACNET) [10.1]. In particular, ASTA uses a standalone modified TCLK system called NMLCLK for the distribution and generation of clock signals and timing signals as shown in Figure 10.1. These signals are distributed throughout the facility and made available to all systems for triggering, arming, data acquisition, and synchronization. The 9 MHz primary reference is provided by the LLRF Master Oscillator and is actually 1300.000/16/9 = 9.0277778 MHz.

The timing system consists of three parts; a rep-rate generator, an event clock generator, and clock receiver/timer modules. The carrier signal is a 9 MHz clock received from the RF master oscillator. The clock generator receives encoded event triggers from a repetition rate generator that is synchronized to the AC power line. The rep-rate generator provides rates of 10 Hz, 5 Hz, 2.5 Hz, 2 Hz, 1 Hz, 0.5 Hz, 0.2 Hz, and 0.1 Hz to accommodate various modes of operation. A timer module, incorporated into the clock generator, can also provide delayed event triggers. By design, all event triggers are generated synchronous with the master oscillator 9 MHz time base and are coherent with the fundamental 10 Hz event. There are 32 clock events available. Of these, 8 have been assigned permanent functionality, as shown in Table 10.1. Currently, variable rate event $AB is used for cryomodule commissioning and variable rate event $AC is used for RF gun commissioning.

The timer modules consist of a clock decoder and eight independent delay timers. Each timer has an associated register for delay, output pulse width, and event reference. Additionally, each timer module provides 3 MHz and 1 MHz pulse trains synchronous to the 9 MHz carrier. These modules typically provide triggers for the klystron modulator, RF , interlocks, and instrumentation in general. Timer output jitter relative to the master oscillator 9 MHz has been measured at $\leq$ 1 nsec.

A small subset of TCLK events is included in NMLCLK to accommodate ACNET console applications. A network multicast of NMLCLK events provides soft real-time information to ACNET user applications and central service processes.

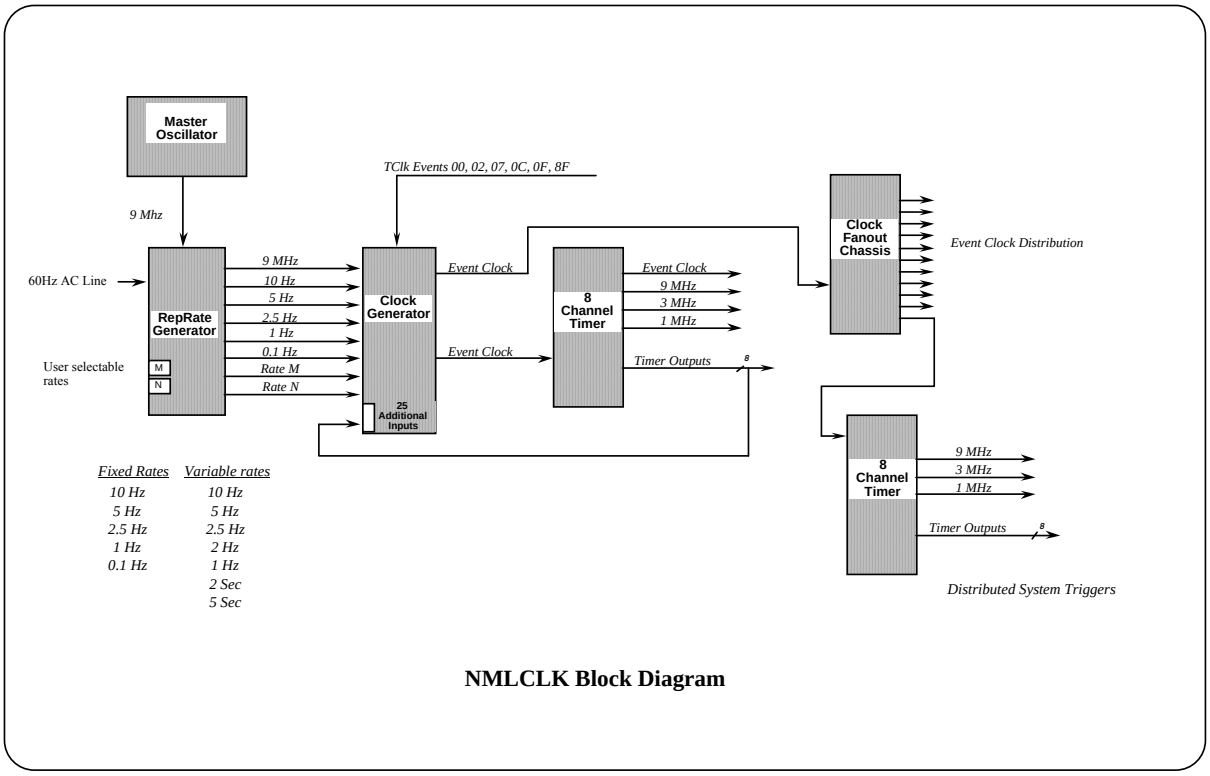

NMLCLK Block Diagram

Figure 10.1: NMLCLK block diagram for ASTA

Table 10.1: Current NMLCLK event usage at ASTA.

Event	Source	System	Delay Name	Description
$00	TCLK			Super Cycle and Master Clock Reset";marks start of supercycle
$02	TCLK			"Time Plot Timestamp Reset":generated every 5 seconds
$07	TCLK			"720 Hz"; poorly synchronized to AC line; permanently enabled
$0C	TCLK			"15 Hz" synchronized to GMPS BMIN Delayed
$0F	TCLK			"15 Hz"; synchronized to A phase of AC line in MAC room
$8F	TCLK			"1 Hz"; Generated by GPS RCVR in computer room
$A0	IP-177	NML/ASTA	none	delayed 2 ms from $AE for laser room triggers
$A1	CM RF	NML/ASTA	none	Cryomodule RF Present, Klystron 6
$A9	RRG	NML/ASTA		"0.1 Hz"; synchronized to AC line and RF Master Oscillator, triggered by Rep-Rate Generator
$AA	RRG	NML/ASTA		"1 Hz"; synchronized to AC line and RF Master Oscillator, triggered by Rep-Rate Generator
$AB	RRG	NML/ASTA		Rate N"; synchronized to AC line and RF Master Oscillator, triggered by Rep-Rate Generator; Cryomodule Commissioning Selectable rate: 0.2, 0.5, 1, 2, 2.5, 5, or 10Hz;
$AC	RRG	NML/ASTA		Rate M"; synchronized to AC line and RF Master Oscillator, triggered by Rep-Rate Generator; RF Gun Commissioning Selectable rate: 0.2, 0.5, 1, 2, 2.5, 5, or 10Hz;

$AD	RRG	NML/ASTA		"2.5 Hz"; synchronized to AC line and RF Master Oscillator, triggered by Rep-Rate Generator
$AE	RRG	NML/ASTA		"5 Hz"; synchronized to AC line and RF Master Oscillator, triggered by Rep-Rate Generator
$AF	RRG	NML/ASTA		"10 Hz"; synchronized to AC line and RF Master Oscillator, triggered by Rep-Rate Generator

References

[10.1] K. Cahill, *et al.*, "The Fermilab Accelerator Controls System", in The ICFA Beam Dyn. Newsletter **47**, p106-124 (2008); (http://lss.fnal.gov/archive/preprint/fermilab-pub-08-605-ad.shtml)

11 Cryogenic system

An economical solution for preparing the initial cryogenics for ASTA was to repurpose equipment from the Tevatron Collider and Fixed Target programs [11.1]. A single Tevatron Satellite Refrigerator was first installed into NML for initial commissioning. A second Tevatron Satellite Refrigerator was added prior to the installation of the first Type III$^+$ cryomodule. In 2010 ARRA funding was used to build a Cryomodule Test Facility (CMTF) next to NML. A new 2°K cryogenic plant is on order for this multipurpose facility. In addition, a 4°K refrigerator from SLAC was repurposed for use in CMTF. Excess refrigeration capacity from this facility can be used to boost the capacity of the existing cryogenic system at ASTA with the addition of a cryogenic distribution system between the adjacent buildings.

The Tevatron style satellite refrigerators used in phase I - III are capable of supplying 4.5°K refrigeration and liquefaction. The refrigeration is used to cool static heat loads associated with the distribution system and low temperature cryomodule shields. The 4.5°K liquefaction is further pumped on to produce the required 2°K refrigeration.

- ASTA Cryogenic load expansion
  - 1st phase: One satellite refrigerator
    - Capture Cavity II with a single Type III$^+$ Cryomodule
  - 2nd phase : Two satellite refrigerators
    - Capture Cavity I and II with one Type III$^+$ Cryomodule
  - 3rd phase : Two satellite refrigerators
    - Capture Cavity I and II with two Type III$^+$ Cryomodules
  - 4th phase : Two satellite refrigerators, new cryogenic plant and distribution system
    - Capture Cavity I and II with a RF Unit
  - 5th phase : Two satellite refrigerators, new cryogenic plant and distribution system
    - Capture Cavity I and II with two RF Units

The configuration of the cryogenic system is shown in Figure 11.1.

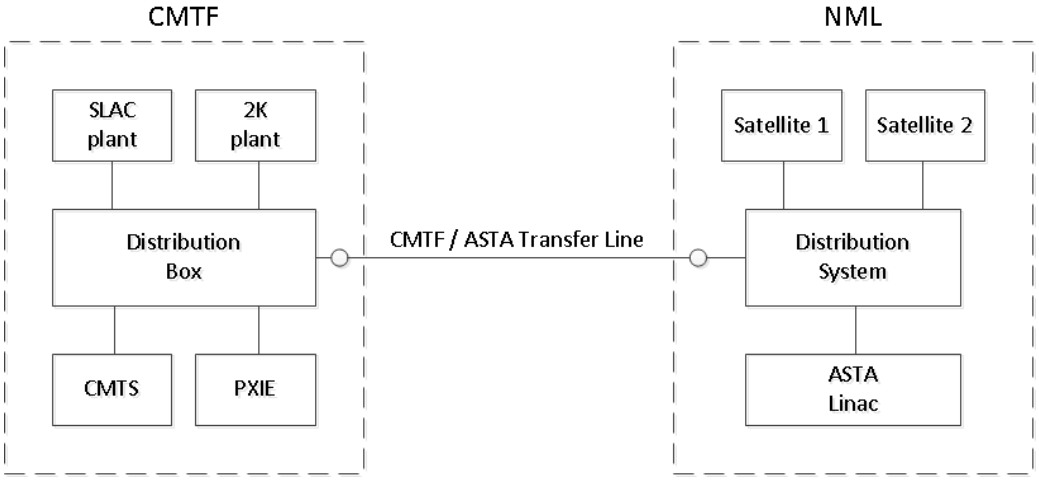

FIGURE 11.1: Cryogenic Configuration at CMTF and NML.

When combined 4.5°K refrigeration and liquefaction capacity is not adequate to cool the load, the repetition rate will need to be lowered from the ILC design of 5 Hz to that which the cryogenic system can support, as shown in Table 11.1.

Table 11.1: Repetition rate limitations at the different cryogenic phases.

ASTA Cryogenic Load Expansion		# of Satellite Refrigerators		New Plant
		1	2	
1	CC-II & One ILC Cryomodule	< 1 Hz	5 Hz	
2	CC-1/II & One ILC Cryomodule	5 Hz	5 Hz	
3	CC-1/II & Two ILC Cryomodules	N/A	5 Hz	
4	CC-1/II & One RF Unit	N/A	< 2 Hz	5 Hz
5	CC-1/II & Two RF Units	N/A	N/A	5 Hz

The current status of cryogenics at the facility is (10/1/12):

- Two satellite refrigerators are operational.
- The SLAC plant is being upgraded for higher pressure operation, new turbines, and a new controls system.
- The CMTF 2°K plant is being fabricated in industry.
- The CMTF to ASTA cryogenic transfer line is under conceptual design.

References

[11.1] A. Martinez, *et al*., "Design and Testing of the New Muon Lab Cryogenic System at Fermilab", in Proceedings of the Cryogenics Engineering Conference and International Cryogenic Materials Conference, June 2010, Tucson, AZ, **AIP Conf. Proc. 1218** p488 (2010); (http://lss.fnal.gov/archive/2009/conf/fermilab-conf-09-566-ad.pdf)

12 Electrical power distribution

12.1 Overview

The NML and CMTF facilities receive electrical power distribution from the FNAL Main Power substation through Feeders #32 and #35 at a distribution potential of 13.8 KV. These feeders supply power to seven 1,500 KVA 480/277 V distribution transformers. Three of these 1,500 KVA transformers supply power to NML and four supply power to the CMTF building. Each transformer feeds a dedicated 2000 A switchboard that supplies 480/277 V 3-phase electrical power for the building and experiment needs. The new electrical distribution system upgrade for the NML/CMTF area was conducted under two separate projects that were started in the summer of 2010 and completed in the summer of 2012. Table 12.1 summarizes the power distribution systems for NML and CMTF.

Table 12.1: NML/CMTF Power distribution transformers

Transformer	Designated Loads
NL-15A	NML – ESB, LCW Pumps, ASTRA Klystron Stations
NL-15B	NML -- Gauge Theory Computational Facility NML Rooms 107&108
NL-15C	NML – LCW Chiller, NML Building HVAC and building utilities
NL-15D	CMTF -- Building Loads, Lighting and Cryogenic Controls
NL-15E	CMTF -- CTI He-Compressor #1, Linde HE-Compressor #1, LCW Chillers
NL-15F	CMTF -- CTI He-Compressor #2, Linde He-Compressor #2, Air Compressor #1
NL-15G	CMTF -- CTI He-Compressor #3, Linde He-Compressor #3, Linde He-Compressor #4, Air Compressor #2

12.2 NML

The first portion of the new electrical distribution at the NML/CMTF campus was undertaken starting in June 2010. The “NML Utilities Upgrade” project (FNAL FESS Project 8-2-188) replaced two aging 30-year-old 1500 A Switchboards powered by FNAL Transformer NL-10 and NL-13 located in the lower level of NML. The switchboard NL-13 had been destroyed in an inundation incident caused by excessive rains on 14Sept09. Water flowing into the switchboard from the incoming conduits caused irreparable damage to the switchboard NL-13. The utilities upgrades for the NML building were planned in a manner that would prevent a recurrence of a similar water inundation problem. The new ground-level location for the two NML replacement switchboards selected on the first floor of NML allowed for all power conduits incoming from the transformer to be terminated above grade and to be routed to the outside of the NML foundation wall in order to prevent water from entering the switchboards. The power outage resulting from the NL-13 switchboard failure also demonstrated the need for a generator back-up power source that would be capable of running the two sump-pumps in the NML High Bay. The Utilities Upgrade project also included a diesel-powered 150 KW generator with automatic cutover capability that will power critical systems for the NML building such as

pumps, lighting, overhead crane, cryogenic systems control and limited critical experiment system loads.

Power to the NML building is supplied by three transformers and switchboards: NL-15A, NL-15B, and NL-15C (Figures 12.1 and 12.2). Transformer and switchboard NL-15B powers the Gauge Theory Computational Center in NML Rooms 107/108 exclusively and it is not available for loads external to that project. Transformer and switchboard NL-15A provides power to building loads, ASTRA experimental loads, two ASTRA 5-MW klystron stations, the NML LCW (Low Conductivity Water) system and pumps, and all ESB (Electrical Service Building) needs. Transformer and switchboard NL-15C provides power to the LCW Chiller system, various NML building power needs such as lighting and HVAC, Cryogenic System power and ASTRA instrumentation rack power.

Figure 12.1: NML switchboards NL15A and NL 15B.

Figure 12.2: Transformers, backup generator and 13.8 KV switch outside the NML building.

12.3 CMTF

The second project that provided significant changes to the NML/CMTF campus power distribution was the CryoModule Test Facility, FESS Project 8-2-189. This project provided a backfeed capability at the termination of 13.8 KV feeders 32 and 35 as well connection to four additional 1,500 kva transformers at CMTF. This capability allows either feeder to supply power to all loads from either feeder #32 or #35 during times of maintenance. Transformer NL-15D was installed and connected as part of the building construction. While the addition of the three transformers NL-15E, NL-15F and NL-15G were installed after beneficial occupancy was received for the CMTF building. These three transformers were removed from locations around the FNAL Tevatron, refurbished, tested, and then installed at the CMTF to power the Micom compressors for the CMTF helium liquefaction plant.

13 Cooling systems

13.1 Low conductivity water systems

The Low Conductivity Water System (LCW) is used to cool various pieces of equipment located at ASTA. All piping and piping fittings are of 304/304L stainless steel, and water is delivered to the equipment at 90°F ±1°F. At the present time there are two VFDs (Variable Frequency Drives) controlling water circulating pumps, each capable of moving 500 GPM at approximately 100 PSIG. These pumps are staged and depending on flow requirements, either one or both pumps can run. A third pump that is to be installed in the near future will be serving as a stand-by pump. In order to remove heat promptly and keep water temperature at 90°F ± 1°F, a 60% water 40% propylene glycol chiller and a plate/frame heat exchanger is used. Three deionizing (DI) bottles polish water to approximately 8 MΩ-cm. There is a series of pressure transducers, temperature transducers, flow meters, etc. all connected to a PLC controlled by a control panel and interfaced to ACNET. Refer to Figure 13.1 for a system diagram.

There are three independent cooling skids as a part of the LCW system, each with its own control panel and connected to ACNET.

- RF Gun Cooling Skid: controls water temperature to within ±0.02°C. This skid operates as an open cooling water loop, which means that LCW is added to the RF Gun Cooling Skid as needed. (refer to Figure 13.2)
- High Energy Dump Cooling Skid: which cools beam absorbers. This skid does not require high temperature stability and controls radioactive water (RAW) temperature to within ±1.0°F. This skid operates as a closed loop system - LCW is separated from Radioactive Water by a stainless steel heat exchanger. (refer to Figure 13.3)
- Low Energy Dump Cooling Skid: This skid does not require high temperature stability either and controls RAW temperature within ±1.0°F. This skid operates as a closed loop system - LCW is separated from RAW by a stainless steel heat exchanger. (refer to Figure 13.3)

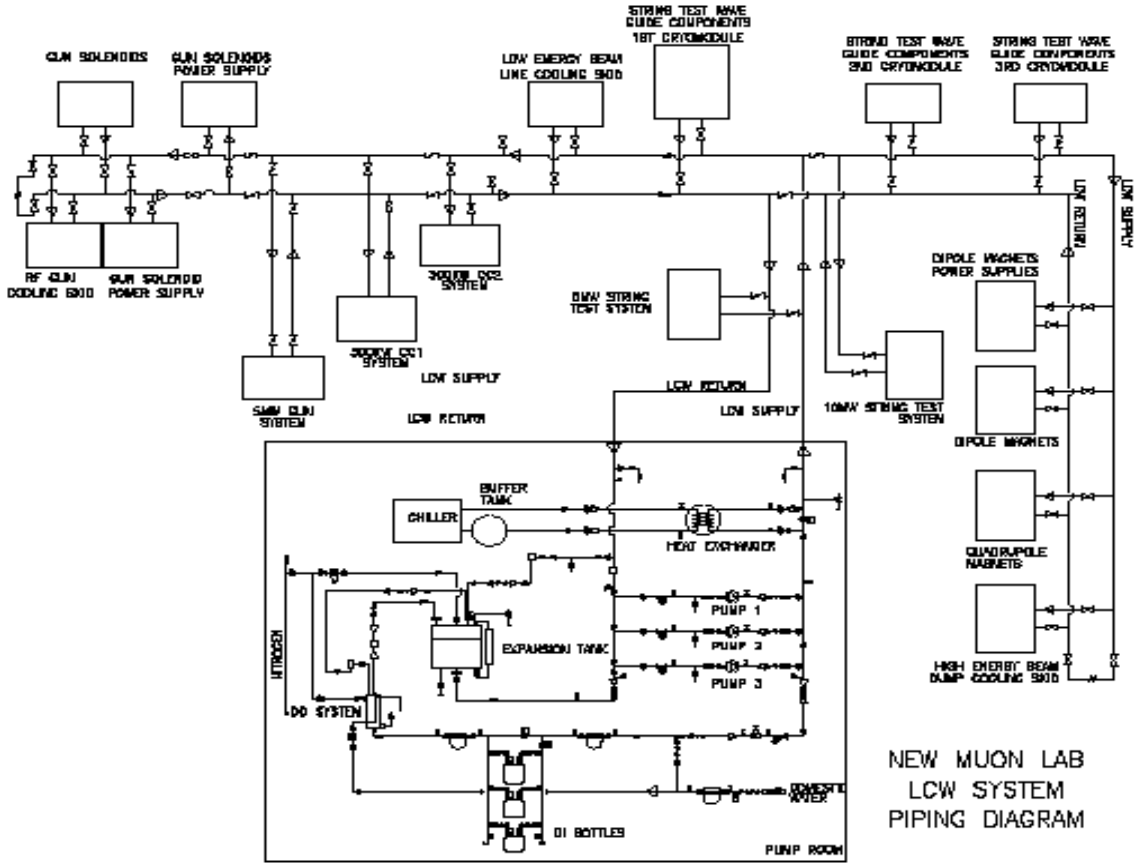

Figure 13.1: Schematic of LCW system.

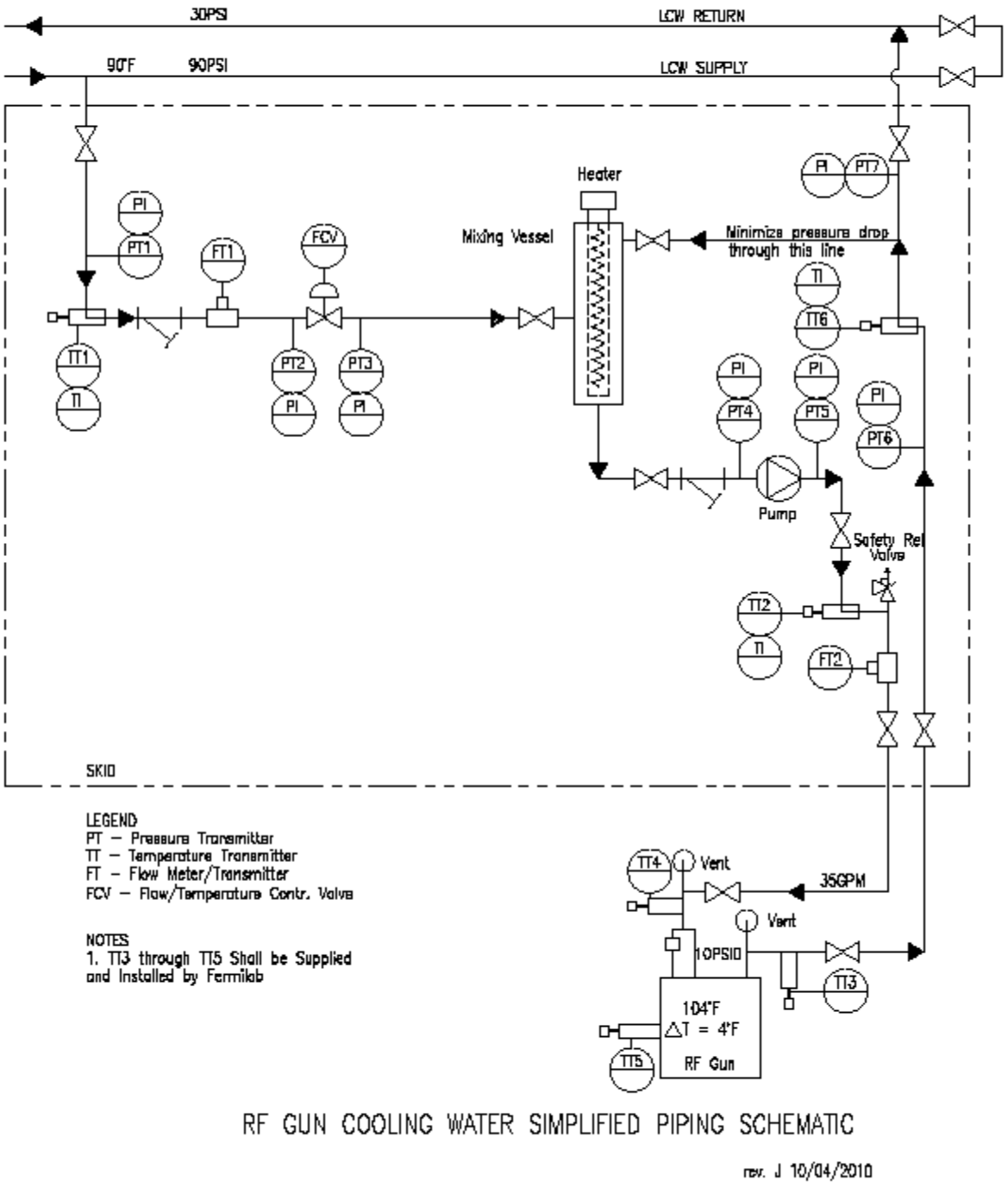

Figure 13.2: RF gun cooling skid schematic.

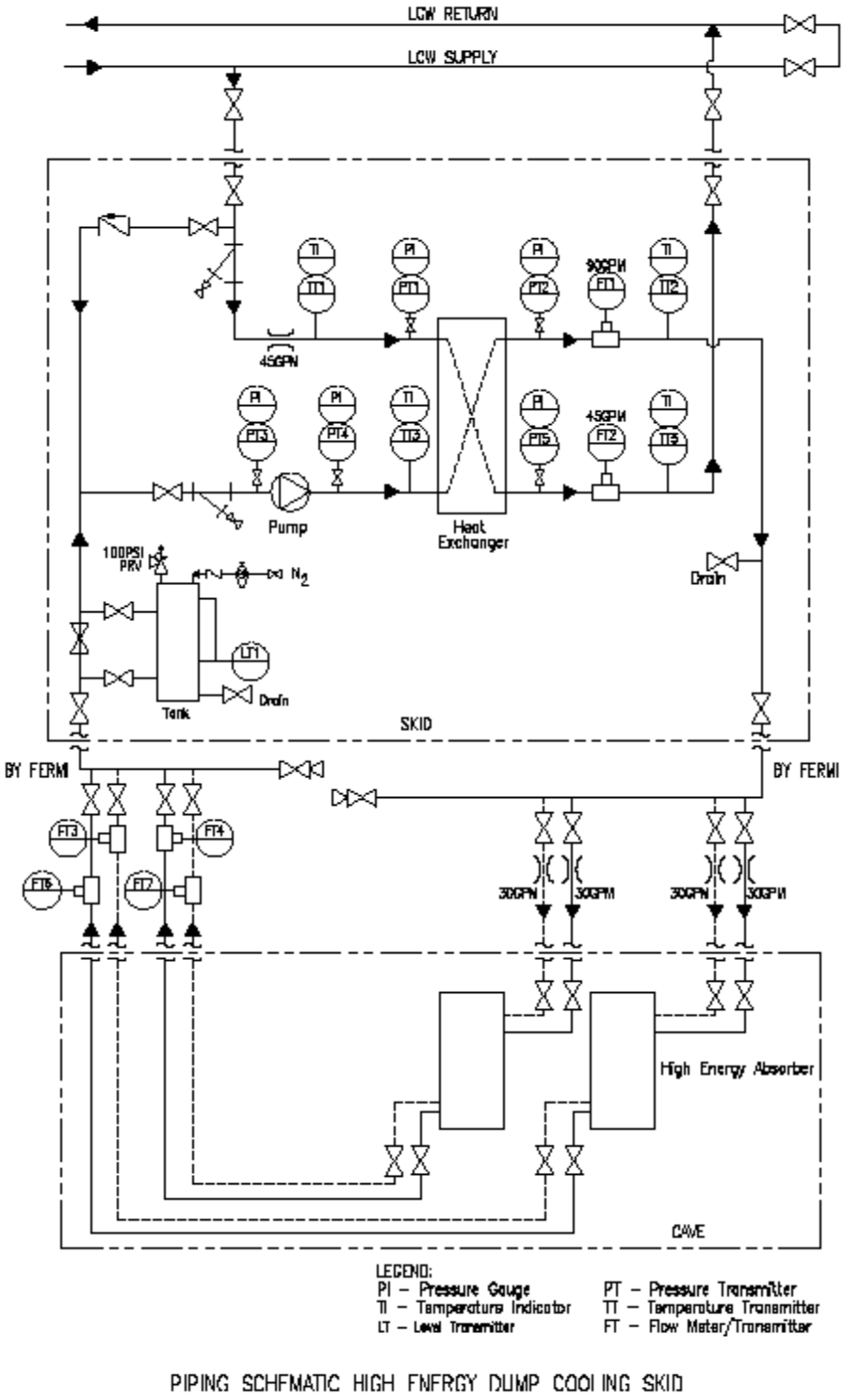

Figure 13.3: Beam absorber cooling skid schematic.

13.2 Industrial cooling water

The industrial cooling water (ICW) is surface water pumped from Casey's Pond and routed through underground piping to various buildings throughout the Fermilab campus for use as fire protection water and process cooling water. The Casey's Pond Pumphouse uses three 400 HP VFD-driven vertical turbine pumps, each rated for 5,000 gpm.

The ICW system in the NML building is used for fire protection and condenser water (heat rejection) for the building's water chiller and the 5-ton HVAC serving the NML laser room, as well as providing available free cooling in winter mode through a plate heat exchanger.

The ICW system in the CMTF buildings is used for fire protection and condenser water (heat rejection) for the cryogenic equipment, sized for the anticipated maximum of 1,600 gpm.

In each building ICW that is utilized for process cooling includes an automatic strainer with automatic backwash. Supply pressure at the buildings is approximately 90 psi and supply temperature varies depending on ambient temperatures.

13.3 HVAC

The NML building HVAC is served by a nominal 115-ton water-cooled twin screw chiller (R-134a Carrier30HXC116) located in the basement mechanical room. The original building chillers were two 150-ton -- one was replaced and the other one is still in place but not operable. This chiller provides ~44°F ICW to the following equipment.

- Two ~30-ton building air handlers
- Six ~3-ton fancoils

The NML building also houses the LCC (Lattice Computer Center) on the main floor. This space is served by a separate ICW system -- CRAC (computer room air conditioner) units with outdoor condensing units at the east side of the parking space. There are, however, two 30-ton CRAC units for the LCC room that are connected to the NML ICW but are not used.

The NML laser room is served by a 5-ton watercooled DX (R-407c) HVAC (Liebert BU07) unit with digital scroll compressor, infrared humidification and SCR reheat.

The NML high bay has a 3,000 cfm make-up air unit (DX-cooling and gas heat) that is enabled during ODH conditions or during tunnel occupancy. This is interlocked with tunnel supply fans and ODH exhaust fans.

The Electrical Service Building (ESB) above the high energy beamline tunnel will be served with two 5-ton wall unit DX HVAC (Marvair), of which one is currently installed. The ESB laser room will be similar to the NML laser room in load and size except it will be a split system DX.

Table 13.1: The given room criteria for each space.

March 16 2009	Exist	Project #1 **(ARRA)**			Project#2		Project#3		
CRITERIA ITEMS	**Existing NML Building**	**Tunnel Extension (below grade)**	**Dump Area**	**Laser Room (NML)**	**Rack Building (ESB)**	**Laser Room (ESB)**	**Cryomodule Test Facility**	**Clean Room**	**Cryo Plant**
HVAC	Existing 78 to 80F summer / 68F winter	No Environmental Requirement.		70 F +/- 0.5F (min 30% RH)	78Fdb +/- 5 F; 50%RH max; No min humidity	70 F +/- 0.5F (min 30% RH)	78Fdb +/- 5 F; 50%RH max; No min humidity	(68 F +/- 2F)	Ambient ventilation and heating (68F min)

The CMTF high bay is served by a nominal 70-ton (27,000 cfm) rooftop type (R-410aDX cool/ gas heat) HVAC unit located outside the building at the north end. The system is configured as a single zone VAV (variable air volume) system and provides 78°F to 80°F cooling / 68°F heating for general space temperatures. The unit is sized to an anticipated equipment load of 42 KW. Two 10 KW supplemental unit heaters are provided near the overhead doors. The CMTF high bay also includes four 11,000 cfm roof exhaust fans and two 5,800 cfm wall exhaust fans for ODH conditions.

The CMTF office area is served by a nominal a 5-ton (2,000 cfm) split type (R-410aDX cool/ gas heat) HVAC unit located on the mezzanine. The system is configured as a single zone constant volume, and provides 75°F to 76°F cooling / 70°F heating for general office temperature control.